ECN

Energy research Centre of the Netherlands

Control design based on aero-hydro-servo-elastic linear models from TURBU (ECN)

T.G. van Engelen

This report has been presented at the EWEC2007 conference, 7-10 May, Milan, Italy

ECN-M--07-054

Control design based on aero-hydro-servo-elastic linear models from TURBU (ECN)

T.G. van Engelen

Energy research Centre of the Netherlands (ECN), Wind Energy
P.O. Box 1, NL-1755 ZG Petten, The Netherlands
telephone: +31 224 564141, telefax: +31 224 568214
email: vanengelen@ecn.nl

Abstract

The ECN computer code TURBU generates elaborate linearised models for 3-bladed wind turbines. These models include the relevant features for control design and aeroealastic stability analysis; they are very well workable because of modally reduced blade tower models. Control loops for blade and tower load reduction were designed for a typical multi-MW wind turbine. A TURBU model was used for analytic examination of the closed loop performance and stability. These 'closed loop predictions' appeared valid when the control loops were evaluated in non-linear time domain simulation. These simulations showed significant load reduction and good closed loop stabilty. The fatigue loads in full load operation were reduced by 10% to 30% for the rotor blades and 4% to 6% for the tower.

Keywords: control design model, closed loop aeroelastic analysis, transfer functions, load reduction.

1 Introduction

The integrated assessment of control and aeroelastic stability for modern and future multi-MW turbine requires the availability of tools that combine accurate structural models with the capability of transfer function analysis. The ECN computer code TURBU has been developed with this in mind. Initially, the development of TURBU was focussed on load calculation for offshore wind turbines in the frequency domain, based on earlier work of Dragt [1], [2]. Preliminary load calculations with TURBU and the layout of the model were presented on the EWEC 2004 in London [3].

TURBU is programmed in the MATLAB programming language [4]. It generates a complete linearised aerohydro-elastic model with control, wave and wind inputs for 3-bladed wind turbines. The approach is similar to that adopted by McCoy [5]. However, TURBU allows for very accurate aeroelastic modelling by enabling prebend, shear offset and unsteady aerodynamics and by taking into account the average deformation. In addition, it allows for order reduction in the structural models and it is strongly based on a modular approach, which facilitates convenient implementation of extensions in future. Finally, TURBU is a stand-alone computer program.

The first part of this paper is dedicated to the composition of the model. Together with appendix A, this part gives a complete explanation of the model, which exceeds by far the description in [3]. Addressed items are:

- components and underlying model equations;
- non-linear solution of the equilibrium state;
- linear model equations and integration to a dynamic wind turbine model.

The second part deals with the use of the model for control design. Addressed items are

- pitch servo behaviour;
- synthesis of feedback structures;
- closed loop transfer functions;
- non-linear time-domain evaluation.

2 Component modelling

In TURBU Offshore a modularised set-up is obtained by idealising the wind turbine to an assemblage of distinct substructures or *components* – the tower/nacelle, the drive train, and the blades – which in turn consist of one or more discrete, rigid elements (see figure 1). This modularisation enables to include control loops and to deal with special features like a (free) flapping hinge and dynamic yawing in a well organised and unconstrained way. Figure 1 shows in the right-hand under corner, on the basis of the fore-aft tower deformation, that the mechanical modelling is based on a co-rotational formulation for beam elements. See a.o. [7] and [8] for this subject. Each element has a local coordinate system. The orientation of this coordinate system results from all (bottom-up) foregoing angular displacements and the local additive angular displacements. The latter occur in the entry point of the concerning element.

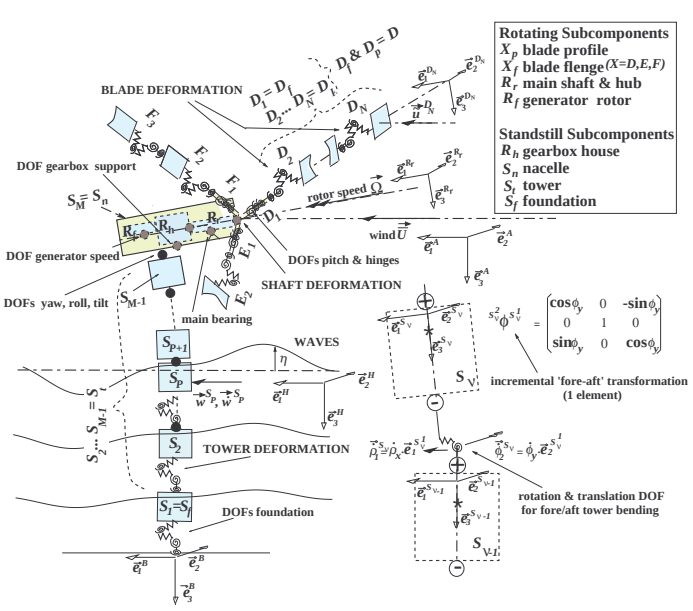

Figure 1: *Assemblage of substructures from elements*

These entry points also may accommodate degrees of freedom (DOFs) for linear displacements. The span from the entry point *after* the DOFs to the exit point of an element is a rigid bar (undeformable). The bending and torsion behaviour of the tower and rotor blades is modelled via these rigid elements with DOFs in the entry points for springs and dampers.

Componenent models are created for the rotor blades, the drive-train, and the support structure. Next to DOFs for bending and torsion, the rotor blades allow DOFs for flap- and leadwise hinges, full span blade pitching, and dynamic setting of the profile coefficients (unsteady aerodynamics). Also additional support structure DOFs apply; for roll, tilt and yaw of the nacelle, and the corresponding translations, as well as for full flexibility of the foundation. DOFs in the drive-train allow for torsion and bending of the rotor shaft, constrained by a main bearing, for rotor speed variation, and for co-axial gearbox house rotation.

Also the behaviour of the wake is accommodated in a 'component model', in which the axial and tangential induction speeds in the rotor annuli are the DOFs.

2.1 Rotor blade model

Each rotor blade is modelled via an assemblage of four submodels. Consider the model for the rotor blade D as depicted in figure 2.

Two of the submodels, typed as D_f and D_p, model

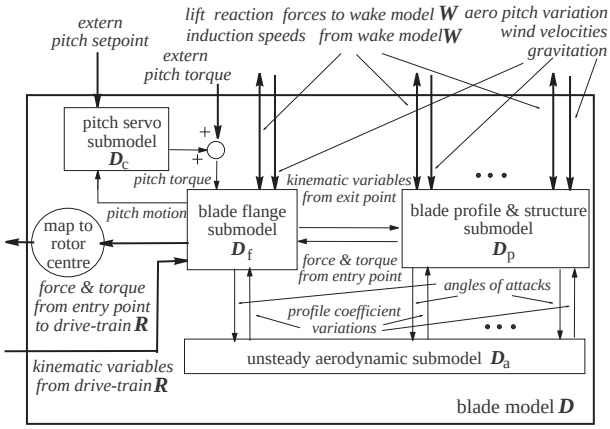

Figure 2: *Blade model as assemblage of submodels*

the structural and quasi-steady aerodynamic behaviour of the blade flange and the blade profile & structure. The (structural) blade model consists of N elements: one element models the flange behaviour via submodel D_f; the remaining $N-1$ elements model the deformation behaviour of the rotor blade via submodel D_p (typical $N = 14$). All N blade elements are loaded by concentrated gravity forces and aerodynamic forces and torques. The remaining two submodels, typed as D_c and D_a, model the full-span pitch servo actuator and the unsteady aerodynamic behaviour.

The pitch actuator submodel D_c emits a pitching torque to the flange D_f. This pitching torque acts as a *responsive* torque in the entry point of D_f, that is to say it acts in opposite direction upon the drive-train R.

The unsteady aerodynamics submodel D_a provides dynamic additions to the aerodynamic profile coefficients for all N blade elements.

The underlying model equations for the flange and profile & structure, the pitch servo actuator and the unsteady aerodynamic conversion are given in appendix sections A.1.1 A.1.2 and A.1.3.

2.2 Drive-train model

The drive-train is modelled via submodels R_f and R_r for the generator rotor and the rotor shaft & hub. Figure 3 shows the interactions of the drive-train model R with the support structure, rotor blades and the environment.

The rotor shaft & hub R_r is loaded by a concentrated gravity force and by the force and torques from the rotor blades in the rotor centre R_r^c. The rotor centre is the location on the shaft axis with the shortest distance to the centre of the pitch

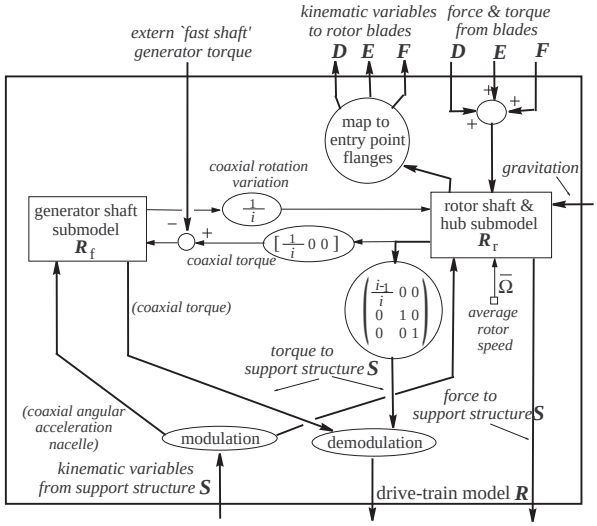

Figure 3: *Drive-train as assemblage of submodels*

bearing.

The mass and inertia moments of the rotating part of the gearbox are added to the masses of the shaft & hub. The transmission ratio i_{gb} of the gearbox governs that the fraction $1/i_{\mathrm{gb}}$ of the outgoing co-axial torque is fed into the generator rotor R_{f}. The remaining outgoing loads are transmitted to the gearbox house. All load exchange for R_{r} is assumed to occur in the rotor centre. In subsection A.2.1 it is clarified that this is allowed under the assumption of rigid nacelle behaviour.

An extern (co-axial) generator torque is emitted to the generator rotor R_{f}. This torque acts as a *responsive* torque that facilitates variable speed operation; it acts in opposite direction upon the support structure S. Since the load exchange for R_{f} only concerns a torque, it may be located anywhere under the assumption of rigid nacelle behaviour; we chose the rotor centre for this (fast shaft) torque loading. The mass and non-coaxial inertia moments of R_{f} are added to those of the nacelle S_{n}.

The underlying model equations for the rotor shaft & hub and the generator rotor are are given in appendix sections A.2.1 and A.2.2.

2.3 Support structure model

The support structure is modelled via four submodels. The two submodels S_{f} and S_{t} establish the structural and hydrodynamic behaviour of the tower just as the flange and blade & profile submodels D_{f} and D_{p} cater for the strucutral and aerodynamic behaviour of the rotor blade D. The ond-element submodel S_{n} is used for including the nacelle. Finally, the gearbox house is a non-rotating subcomponent and is added as the fourth submodel to the support structure. Since it physically belongs to the drive-train it is typed R_{h}.

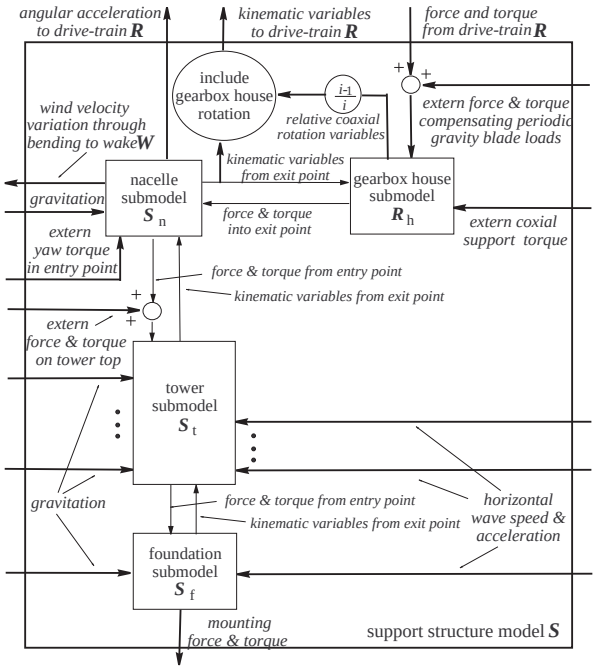

Figure 4: *Support structure as assemblage of submodels*

The (structural) support structure model consists of M elements (gearbox house *not* included): the first element models the foundation behaviour via submodel S_{f}, the elements 2 up to $M-1$ model the deformation behaviour of the tower via submodel S_{t}, and the last element models the nacelle behaviour via submodel S_{n} (typical $M = 15$). All M blade elements are loaded by concentrated gravity forces. For an offshore turbine, the underwater tower elements and the foundation element are also loaded by concentrated hydrodynamic forces and torques.

The gearbox house R_{h} just feeds through all loads from the drive-train except the co-axial torque. An extern co-axial support torque is emitted to the gearbox house R_{h}, which facilitates gearbox house rotation; this torque acts as a *responsive* torque and acts in opposite direction upon the nacelle. The mass and inertia moments of R_{h} are added to those of the nacelle S_{n}.

An extern yawing torque is emitted to the nacelle S_{n}. This *responsive* torque facilitates dynamic yawing; it acts in opposite direction upon the top of the tower S_{t}.

Forces and torques in three directions can be added as *independent loading* on the gearbox house, located in the rotor centre. These are *non*-responsive loads; they are to be considered as loads such as caused by the wind or gravitation. TURBU provides values for these loads that just compensate for the *average* gravitation loads in the standstill frame, average loads that result from the periodic gravity loading of the blades in the rotating frame.

Forces and torques in three directions can also be added as *independent* loading on the tower, located in the centre of the tower top (= yaw bearing centre). These *non*-responsive loads can be used for simulation of damper devices in the tower top. It must be remarked that all reaction loads on these devices as well as the inertia effects *perpendicular to their effecutation orientation* are not included in the structural behaviour of the support structure.

The underlying model equations for the gearox house, nacelle, and tower and foundation are are given in appendix sections A.3.1, A.3.2, and A.3.3.

2.4 Wake model

The modelling of the induction behaviour is based on Blade Element Momentum theory (BEM), as described in [11]. The steady state behaviour is extended with Prandtl's correction to account for the influence of the wake. Corrections to the 2D lift polar that account for 3D-effects are not included in TURBU and thus have to be performed beforehand and added to the input files with lift polars.

The dynamic wake behaviour is accounted for via the ECN Differential Equation model for dynamic inflow as described in [15] and verified in [14]. In this way only the transient behaviour of the rotor-annulus uniform induction speed is included. In figure 2 it has been shown that the reaction forces of the lift forces on the rotor blades are interaction input signals to the wake model; extern input signals are the axial, lateral and vertical wind speed coordinates in the intersections of the blade elements with annuli in the wake. The wake model provides the annulus-uniform axial and tangential induction speeds to the rotor blade elements.

The underlying BEM-based model equations are described in appendix section A.4.

3 Equilibrium conditions

Since TURBU is used for linear analysis, the equilibrium conditions have to be determined before the linear model formulation can be established.

The driving variables for the equilibrium conditions are the mean values of the wind speed, the rotational speed, yaw misalignment angle and the pitch angles; the latter are assumed to be equal for the three rotor blades. The variables that define the equilibrium conditions are

- equilibrium driving variables;
- mean induction speeds in the rotor annuli;
- mean values of angular and linear DOFs

Actually, the mean yaw angle misalignment and pitch angles define the mean values of the yaw-oriented DOF in the nacelle and the pitch-oriented DOF in the flange of the blades. All mean loads on the wind turbine and mean displacements are derived from these equilibrium defining variables. In TURBU an iteration procedure has been implemented for the determination of the equilibrium. Each iteration consists of four steps.

The iteration procedure is preceeded by setting the mean values of the angular DOFs of the blades equal to the *configuration* values, derived from the cone and pitch angle and skewness and prebend specifications. The mean values of the angular DOFs of the drive-train and support structure, as well as the mean values of all linear DOFs are set equal 0. The mean deformation values of all DOFs are initially set to 0. The sum of the configuration and the mean deformation values of the DOFs set up the average shape of the components.

The following four calculation steps are performed sequentially in each iteration:

- solution of the BEM-equations that yield the axial and tangential induction speed values in the rotor annuli for the rotor layout that belongs to the lately determined average shape of the rotor, drive-train and support structure (equation (72));
- solution of the steady-state rotor blade impulse equations that yield the mean *deformation* values of the angular and linear DOFs for the lately determined induction state of the rotor annuli and average shape of drive-train and support structure (equation (25); non-zero average accelerations in the rotating-frame);
- solution of the steady-state drive-train impulse equations that yield the mean *defor-*

mation values of the co-axial DOFs for the rotor loading that belongs to the lately determined induction state and average shape of rotor and support structure (equation (54));

- solution of the steady-state support structure impulse equations that yield the mean *deformation* values of the angular and linear DOFs for the loading that belongs to the lately determined induction state and average shape of the rotor and drive-train (equation (64));

All solution procedures except that for the the drive-train consist of iteration procedures by theirselves.

The solution procedure for the BEM-equations may also be directed by the user to calculate the required pitch angle for achieving nominal power. The equilibrium driving parameter then is the nominal power instead of the pitch angle. In that case the BEM solution procedure consists of nested iterations in which the outer loop is governed by pitch angle search.

Because of axi-symmetry the mean values of the bending DOFs of the drive-train remain 0.

The overall procedure appears to work well for very flexible blades too. For slapstick blades convergence problems arise, but these are not expected to be realistic.

4 Integrated dynamic model

The integrated dynamic model is set up by coupled differential equations that describe the behaviour of the rotor blades, the drive-train, the support structure and the wake around the equilibrium state. First is described how the required formulations for the component models are obtained from the model equations derived in section 2. Afterwards the merging procedure for the component models is explained, which includes the connection of the different models and the transformation to fixed-frame coordinates. Finally, the reduction of the model order is described.

4.1 Component models

The dynamic component models are to be formulated as linear first order state space representations. This enables to link them together in a convenient way. The linear dynamic behaviour and the mapping of input to output variables is then described by the following matrix-vector equations:

$$\begin{aligned} \frac{\mathrm{d}}{\mathrm{d}t}\left(\underline{z}\right) &= \boldsymbol{A}\cdot\underline{z}+\boldsymbol{B}\cdot\underline{v} \\ \underline{y} &= \boldsymbol{C}\cdot\underline{z}+\boldsymbol{K}\cdot\underline{v} \end{aligned}$$

Vectors $\underline{v}$, $\underline{z}$ and $\underline{y}$ respectively contain the inputs, state variables and outputs (all variations). Matrices $\boldsymbol{A},\boldsymbol{B},\boldsymbol{C}$ and $\boldsymbol{K}$ are the transition, input, output and feedthrough matrix.

The next four paragraphs describe the building of the state space representations for the dynamic behaviour of the rotor blades, the drive-train, the support structure and the wake.

4.1.1 State space model & submodels rotor blade

The submodels of the blade flange D_{f} and profile & structure D_{p} are derived from the normal differential vector equations by equation (25). To this aim, we have to formulate the edge, flat and pitch oriented coordinates of these vector equations along the best possible approximations of the true axes for edge-, flat- and pitch-wise deformation. It is along *these* axes that the viscoelastic responsive loads in correspondence with equation (33) apply.

The coordinates in equation (25) pertain to the

$\Rightarrow$ *final* coordinate system $\vec{e}^{\,D_3}_{(x,y,z)}$,

which originates from $\vec{e}^{\,D_2}_{(x,y,z)}$ through subsequent rotation over

- pitch angle $\phi_1^{D_3}$ along the y-axis;
- flatwise angle $\phi_2^{D_3}$ along the z-axis;
- edgewise angle $\phi_3^{D_3}$ along the x-axis.

Remember the bottom-up ranking 'pitch-flat-edge' in the blade elements as mentioned in §2.1.

Note that the z-axis and x-axis for the flat- and edgewise rotation belong to the

$\Rightarrow$ *intermediate* coordinate systems $\vec{e}^{\,D_3^1}_{(x,y,z)}$, $\vec{e}^{\,D_3^2}_{(x,y,z)}$,

which are obtained by rotating $\vec{e}^{\,D_2}_{(x,y,z)}$ and $\vec{e}^{\,D_3^1}_{(x,y,z)}$ over the pitch angle and flatwise angle respectively.

These considerations imply the following links between the orientation of the deformations and the coordinate system axes along which the belonging (scalar) differential equations are to be derived:

- co-axial angular and linear along $\vec{e}_y^{\,D_2}$
- flatwise angular and linear along $\vec{e}_z^{\,D_3^1}$ and $\vec{e}_x^{\,D_3^1}$;

- edgewise angular and linear along $\vec{e}_x^{\,D_3^2}$ and $\vec{e}_z^{\,D_3^2}$;

Now, we lump together the torque and force loads in equation (25) to $\underline{t}^{D_3^{\ominus}}$ and $\underline{f}^{D_3^{\ominus}}$. The differential equations for the dynamic behaviour related to the angular and linear flatwise deformation around the equilibrium is then obtained from the following scalar equalities:

$$\begin{aligned}\left(\delta({}^{D_3^1}\Phi^{D_3}\cdot({}^{D_3^{\ominus}}\dot{\underline{h}}^{D_3}-\underline{t}^{D_3^{\ominus}}))\right)_z=0 \quad\Leftrightarrow\quad \delta\dot{h}_{\mathrm{eq}_z}^{D_3}=0\\ \left(\delta({}^{D_3^1}\Phi^{D_3}\cdot(\underline{\dot{p}}^{D_3}-\underline{f}^{D_3^{\ominus}})\right)_x=0 \quad\Leftrightarrow\quad \delta\dot{p}_{\mathrm{eq}_x}^{D_3}=0\end{aligned} \tag{1}$$

For the backward transformation matrix ${}^{D_3^1}\Phi^{D_3}$ holds (see also equation (23)):

$$\begin{aligned}{}^{D_3^1}\Phi^{D_3} \;=\; &\Phi_{\mathrm{z}}^{\mathrm{T}}(\bar{\phi}_2^{D_3})\cdot\Phi_{\mathrm{x}}^{\mathrm{T}}(\bar{\phi}_3^{D_3})-\Phi_{\mathrm{z}}^{\mathrm{T}}(\bar{\phi}_2^{D_3})\cdot\\ &\tfrac{\mathrm{d}\Phi_{\mathrm{x}}^{\mathrm{T}}}{\mathrm{d}\phi}((\bar{\phi}_3^{D_3})\cdot\delta\phi_3^{D_3}-\tfrac{\mathrm{d}\Phi_{\mathrm{z}}^{\mathrm{T}}}{\mathrm{d}\phi}(\bar{\phi}_2^{D_3})\cdot\Phi_{\mathrm{x}}^{\mathrm{T}}(\bar{\phi}_3^{D_3})\cdot\delta\phi_2^{D_3}\end{aligned} \tag{2}$$

The belonging 'flatwise' differential equations are obtained by linear expansion of the equalities in equation (1). This yields second order differential equations in variations $\underline{\varphi}^D$ and $\underline{\varrho}^D$ of the blade's DOF-vectors driven by variations $\underline{v}^{D_\mathrm{P}}$ of the input variables to the blade & profile submodel (use short forms $\delta\dot{h}_{\mathrm{eq}_z}^{D_3}$ and $\delta\dot{p}_{\mathrm{eq}_x}^{D_3}$ and omit prefix δ):

$$\begin{aligned}\frac{\partial\dot{h}_{\mathrm{eq}_z}^{D_3}}{\partial\begin{bmatrix}\underline{\ddot{\varphi}}\\ \underline{\ddot{\varrho}}\end{bmatrix}}\begin{bmatrix}\underline{\ddot{\varphi}}^D\\ \underline{\ddot{\varrho}}^D\end{bmatrix}+\frac{\partial\dot{h}_{\mathrm{eq}_z}^{D_3}}{\partial\begin{bmatrix}\underline{\dot{\varphi}}\\ \underline{\dot{\varrho}}\end{bmatrix}}\begin{bmatrix}\underline{\dot{\varphi}}^D\\ \underline{\dot{\varrho}}^D\end{bmatrix}+\frac{\partial\dot{h}_{\mathrm{eq}_z}^{D_3}}{\partial\begin{bmatrix}\underline{\varphi}\\ \underline{\varrho}\end{bmatrix}}\begin{bmatrix}\underline{\varphi}^D\\ \underline{\varrho}^D\end{bmatrix}=-\frac{\partial\dot{h}_{\mathrm{eq}_z}^{D_3}}{\partial\underline{v}^{D_\mathrm{P}}}\,\underline{v}^{D_\mathrm{P}}\\ \frac{\partial\dot{p}_{\mathrm{eq}_x}^{D_3}}{\partial\begin{bmatrix}\underline{\ddot{\varphi}}\\ \underline{\ddot{\varrho}}\end{bmatrix}}\begin{bmatrix}\underline{\ddot{\varphi}}^D\\ \underline{\ddot{\varrho}}^D\end{bmatrix}+\frac{\partial\dot{p}_{\mathrm{eq}_x}^{D_3}}{\partial\begin{bmatrix}\underline{\dot{\varphi}}\\ \underline{\dot{\varrho}}\end{bmatrix}}\begin{bmatrix}\underline{\dot{\varphi}}^D\\ \underline{\dot{\varrho}}^D\end{bmatrix}+\frac{\partial\dot{p}_{\mathrm{eq}_x}^{D_3}}{\partial\begin{bmatrix}\underline{\varphi}\\ \underline{\varrho}\end{bmatrix}}\begin{bmatrix}\underline{\varphi}^D\\ \underline{\varrho}^D\end{bmatrix}=-\frac{\partial\dot{p}_{\mathrm{eq}_x}^{D_3}}{\partial\underline{v}^{D_\mathrm{P}}}\,\underline{v}^{D_\mathrm{P}}\end{aligned} \tag{3}$$

The expressions for the two other orientations are obtained in the same way; replace the subscript-pair $\{z,x\}$ by $\{x,z\}$ and by $\{y,y\}$. After these equations have been stacked for the three orientations in D_3, and this has been done for all elements of D_p, the matrix/vector differential equation for D_p is obtained as a mass-damper-spring formulaton:

$$\boldsymbol{M}\cdot\begin{bmatrix}\underline{\ddot{\varphi}}^D\\ \underline{\ddot{\varrho}}^D\end{bmatrix}+\boldsymbol{D}\cdot\begin{bmatrix}\underline{\dot{\varphi}}^D\\ \underline{\dot{\varrho}}^D\end{bmatrix}+\boldsymbol{S}\cdot\begin{bmatrix}\underline{\varphi}^D\\ \underline{\varrho}^D\end{bmatrix}=\boldsymbol{G}\cdot\underline{v}^{D_\mathrm{P}} \tag{4}$$

It should be noted that *those* rows and columns of the matrices $\boldsymbol{M}$, $\boldsymbol{D}$ and $\boldsymbol{S}$ are to be removed which pertain to the angular and linear orientations that are no DOF in the sense of submodel D_p. Thus the first six columns will be removed, since these pertain to the (potential) DOFs in submodel D_f, and also those rows and columns are removed that pertain to the co-axial linear orientation of elements D_2 up to D_N. In input matrix $\boldsymbol{G}$ only the removal of the corresponding *rows* applies.

After the columns and rows have been removed, the mass-damper-spring formulation is a valid model of the structural and quasi-steady aerodynamic behaviour of the blade profile & structure D_p.

The model equations for the output variables of D_p are obtained by the linear expansion of the output vector $\underline{y}^{D_\mathrm{P}}$ in the DOFs and their first and second derivatives and the submodel-input variables. After elimination of the dependency on the second derivatives of the DOFS via the state equations, the following expression for $\underline{y}^{D_\mathrm{P}}$ is obtained:

$$\underline{y}^{D_\mathrm{P}}=\boldsymbol{L}\cdot\begin{bmatrix}\underline{\dot{\varphi}}^D\\ \underline{\dot{\varrho}}^D\end{bmatrix}+\boldsymbol{H}\cdot\begin{bmatrix}\underline{\varphi}^D\\ \underline{\varrho}^D\end{bmatrix}+\boldsymbol{K}\cdot\underline{v}^{D_\mathrm{P}} \tag{5}$$

The same model derivation procedure applies for the flange D_f, although only *one* element applies, viz D_1.

Thus it is explained that for the *structural* submodels of D_f and D_p

- the equations of motion appear as second order differential equations in the DOFs (mass-damper-formulation);
- the output equations map DOFs and their 1st and 2nd time-deriviatives, as well as the submodel-input variables, to the submodel-output variables.

The desired first order state space parametrisation can be easily derived from this formulation. The new state variables are both the DOFs and their 1st time-deriviatives.

The model equations (35) and (36) of the pitch servo actuator (D_c for blade D) are transformed into a state space parametrisation via a standard MATLAB-function.

The equations of motion of the submodel for the unsteady aerodynamic behaviour D_a have been formulated directly as (scalar) first order state equations, combined with output equations in §A.1.3. The output equations map for each blade element the state variable and submodel-input variables to the dynamic addition of the lift-coefficient. The stacking of the state and output equations and rewriting them as matrix-vector products yields the desired first order state space representation.

When the four submodels of the rotor blade D are connected to each other via the interaction

variables according to figure 2, the desired first order state space representation for D is obtained:

$$\begin{aligned} \frac{\mathrm{d}}{\mathrm{d}t}\left(\underline{z}^{D}\right) &= \boldsymbol{A}^{D}\cdot\underline{z}^{D}+\boldsymbol{B}^{D}\cdot\underline{v}^{D} \\ \underline{y}^{D} &= \boldsymbol{C}^{D}\cdot\underline{z}^{D}+\boldsymbol{K}^{D}\cdot\underline{v}^{D} \end{aligned}$$

4.1.2 State space model & submodels drive-train

The two submodels of the drive-train, those of the generator rotor R_{f} and of the rotor shaft & hub R_{r}, pertain both to the structural dynamic behaviour.

The desired first order state space representations are obtained from the 'mass-spring-damper' formulations in the same way as described for the blade flange and profile & structure.

When the two submodels of the drive-train R are connected to each other via the interaction variables according to figure 3, the desired first order state space representation for R is obtained:

$$\begin{aligned} \frac{\mathrm{d}}{\mathrm{d}t}\left(\underline{z}^{R}\right) &= \boldsymbol{A}^{R}\cdot\underline{z}^{R}+\boldsymbol{B}^{R}\cdot\underline{v}^{R} \\ \underline{y}^{R} &= \boldsymbol{C}^{R}\cdot\underline{z}^{R}+\boldsymbol{K}^{R}\cdot\underline{v}^{R} \end{aligned}$$

4.1.3 State space model & submodels support structure

The four submodels of the support structure, those of the gearbox house R_{h}, the nacelle S_{n}, the tower S_{t} and the foundation S_{f}, all pertain to the structural dynamic behaviour.

The desired first order state space representations are obtained from the 'mass-spring-damper' formulations in the same way as described for the blade flange and profile & structure.

When the four submodels of the support structure S are connected to each other via the interaction variables according to figure 4, the desired first order state space representation for S is obtained:

$$\begin{aligned} \frac{\mathrm{d}}{\mathrm{d}t}\left(\underline{z}^{S}\right) &= \boldsymbol{A}^{S}\cdot\underline{z}^{S}+\boldsymbol{B}^{S}\cdot\underline{v}^{S} \\ \underline{y}^{S} &= \boldsymbol{C}^{S}\cdot\underline{z}^{S}+\boldsymbol{K}^{S}\cdot\underline{v}^{S} \end{aligned}$$

4.1.4 State space model wake behaviour

The equations of motion of the 'component' model for the dynamic wake behaviour W have been formulated directly as (scalar) first order state equations. The induction speed variations per annulus are the state variables. The desired first order parametrisation is obtained from the stacking of the scalar state equations and specifying the identity matrix for the output matrix and null matrix for the feedthrough matrix. It is formulated by:

$$\begin{aligned} \frac{\mathrm{d}}{\mathrm{d}t}\left(\underline{z}^{W}\right) &= \boldsymbol{A}^{W}\cdot\underline{z}^{W}+\boldsymbol{B}^{W}\cdot\underline{v}^{W} \\ \underline{y}^{W} &= \boldsymbol{C}^{W}\cdot\underline{z}^{W}+\boldsymbol{K}^{W}\cdot\underline{v}^{W} \end{aligned}$$

4.2 Merging the component models

The first order state space representation allows to automate the connection of the blade and flange model via the interaction input/ouput-relationships; the connection requires lists of index pairs in the input and output vectors. A high rate of genericity is achieved because signal name lists exist for the output and input vectors; each signal name involves the identifier for the destination or source (sub)component. This enables to define the required lists of index pairs from searches on identical signal names in the input and output name lists.

According to the previous section, the modularised linear modelling approach yields state space models for the 3 rotor blades (D, E and F), for the dynamic wake behaviour (W), for the drive train (R) and for the support structure (S). Figure 5 shows the matrix equations for the state space representations of the component models and the interaction signals as well as the exogeneous input signals from the wind and the waves. The interface between the drive-train and support structure involves the rotor azimut angle, which amounts to $\bar{\Omega}t$ in the sense of 'on-average evolution'.

The interface between each rotor blade and the air tube ('wake') does not include a rotation. The orientation of the axial and tangential reaction forces from a blade on the air turbe coincides with the axial and tangential orientation of the air tube in the intersection with that blade. The rotor blades receives the annulus-average axial and tangential induction speed variations.

In general, the equations of motion for the integrated model will have coefficients that are periodic in $\bar{\Omega}t$:

$$\begin{aligned} \dot{\underline{z}} &= \boldsymbol{A}(\bar{\Omega}t)\cdot\underline{z}+\boldsymbol{B}(\bar{\Omega}t)\cdot\underline{v} \\ \underline{y} &= \boldsymbol{C}(\bar{\Omega}t)\cdot\underline{z}+\boldsymbol{K}(\bar{\Omega}t)\cdot\underline{v} \end{aligned} \qquad (6)$$

This makes them not suitable for well-known solution procedures for systems of ordinary first order differential equations. Because of the polar symmetry of rotors with three or more identical blades a simple transformation – the so-called

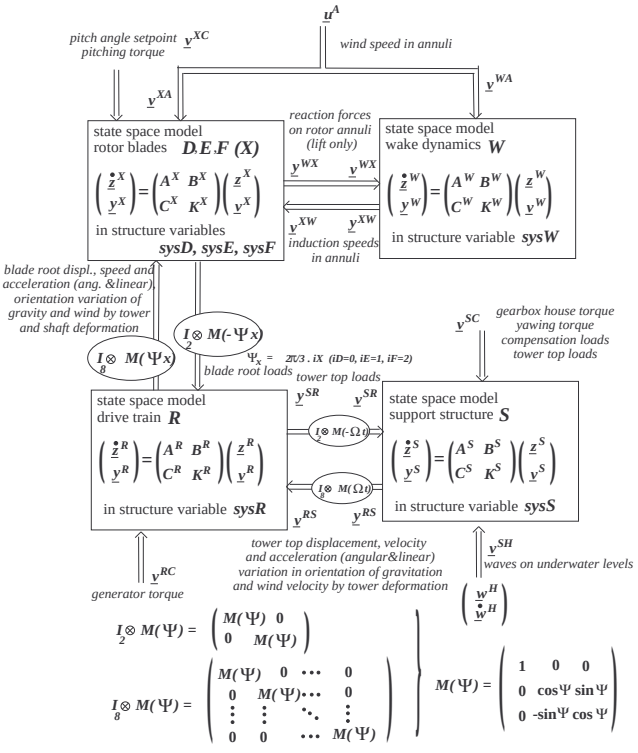

Figure 5: *Interdependency of state space models for the distinct substructures of the wind turbine*

multi-blade transformation, see Coleman & Feingold [21]– can eliminate the periodic coefficients in the full system equations. This transformation is also carried through by Hansen [25] and McCoy [5].

The only price to be payed for it consists in modulation of the wind speed variations before they enter the transformed system equations via input vector $\underline{\epsilon}$ and in modulation of the transformed system output variables in $\underline{\eta}$ in order to retransform them along the desired coordinate systems. The following linear time invariant model formulation with modulated input preprocessing and output postprocessing then applies:

$$\begin{aligned} \underline{\epsilon} &= T_{v_{\mathrm{cm}}}^{-1}(\bar{\Omega}t)\cdot\underline{v} \\ \dot{\underline{q}} &= \boldsymbol{A}_{\mathrm{cm}}\cdot\underline{q}+\boldsymbol{B}_{\mathrm{cm}}\cdot\underline{\epsilon} \\ \underline{\eta} &= \boldsymbol{C}_{\mathrm{cm}}\cdot\underline{q}+\boldsymbol{K}_{\mathrm{cm}}\cdot\underline{\epsilon} \\ \underline{y} &= T_{y_{\mathrm{cm}}}(\bar{\Omega}t)\cdot\underline{\eta} \end{aligned} \tag{7}$$

The invariant input, state transition, output and feedthrough matrix in this model is obtained from the corresponding periodic matrices in the earlier mentioned model via the Coleman transformation matrices $T_{z_{\mathrm{cm}}}(\bar{\Omega}t)$, $T_{v_{\mathrm{cm}}}(\bar{\Omega}t)$ and $T_{y_{\mathrm{cm}}}(\bar{\Omega}t)$ on the state, input and output vector respectively, *by performing the transformation for an arbitrary fixed value of the rotor azimut angle* $\bar{\Omega}t$. The fixed-frame system matrices are obtained as follows from the (partially) rotating system matrices:

$$\begin{aligned} \boldsymbol{A}_{\mathrm{cm}} &= T_{z_{\mathrm{cm}}}^{-1}(\bar{\psi})\cdot\left(\boldsymbol{A}(\bar{\psi})\cdot T_{z_{\mathrm{cm}}}(\bar{\psi})-\dot{T}_{z_{\mathrm{cm}}}(\bar{\psi})\right) \\ \boldsymbol{B}_{\mathrm{cm}} &= T_{z_{\mathrm{cm}}}^{-1}(\bar{\psi})\cdot\boldsymbol{B}(\bar{\psi})\cdot T_{v_{\mathrm{cm}}}(\bar{\psi}) \\ \boldsymbol{C}_{\mathrm{cm}} &= T_{y_{\mathrm{cm}}}^{-1}(\bar{\psi})\cdot\boldsymbol{C}(\bar{\psi})\cdot T_{z_{\mathrm{cm}}}(\bar{\psi}) \\ \boldsymbol{K}_{\mathrm{cm}} &= T_{y_{\mathrm{cm}}}^{-1}(\bar{\psi})\cdot\boldsymbol{K}(\bar{\psi})\cdot T_{v_{\mathrm{cm}}}(\bar{\psi}) \end{aligned} \tag{8}$$

The Coleman transformation involves the mapping of any corresponding quantities on the rotor blades D, E and F to multi-blade coordinates via the 3×3 matrix kernel $T_{\mathrm{ker_X}}$:

$$T_{\mathrm{ker_X}}(\bar{\Omega}t)=\begin{pmatrix} 1 & \sin(\bar{\Omega}t) & \cos(\bar{\Omega}t) \\ 1 & \sin(\bar{\Omega}t+\frac{2}{3}\pi) & \cos(\bar{\Omega}t+\frac{2}{3}\pi) \\ 1 & \sin(\bar{\Omega}t+\frac{4}{3}\pi) & \cos(\bar{\Omega}t+\frac{4}{3}\pi) \end{pmatrix} . \tag{9}$$

It also involves the mapping of x, y and z-coordinates of any vector on the rotor shaft to multi-blade coordinates via the 3×3 matrix kernel $T_{\mathrm{ker_R}}$:

$$T_{\mathrm{ker_R}}(\bar{\Omega}t)=\begin{pmatrix} 1 & 0 & 0 \\ 0 & \cos(\bar{\Omega}t) & \sin(\bar{\Omega}t) \\ 0 & -\sin(\bar{\Omega}t) & \cos(\bar{\Omega}t) \end{pmatrix} . \tag{10}$$

All input and output variables as well as all state variables are accompanied by unique signal names. Each signal name involves the identifier for the destination, source or possessing component for an output, input or state variable respectively. This enables to create in an automated way the appropriate matrix kernels on the right locations in the Coleman transformation matrices for each set of 3 blade variables, each rotor shaft vector variable and each support structure variable.

It should be noted that periodic coefficients due to external forces (gravity and uniform wind loading) are not eliminated by the Coleman transformation. The parametric excitations terms due to gravity and wind loads can generally be ignored for all but extremely flexible blades.

4.2.1 Reduction of the model order

The submodels of the blade profile & structure D_{p} and of the tower S_{t} can be reduced in order. For this we apply the method proposed by Hurty [22], [23], which has been made more easily applicable by Craig & Bampton [24].

The implemented method allows to significantly reduce the degrees of freedom in the blade and tower model without loss of accuracy in the dynamic behaviour of the lower bending modes; the number of modes to be included can be specified. Typically, the order of the integrated model can be reduced from 600 to 100 without any loss of accuracy in frequencies up to 5 Hz or even higher. This enormously accelerates the dynamic analysis.

The implementation was not so straightforward because of the applied submodel connection mechanism.

When submodels are connected in accordance with the schemes proposed by Hurty and Craig & Bampton, the 'inner' boundary dofs vanish from the overall set of equations of motions during the very coupling. These inner boundary dofs *must* be present in the reduced order model so that they can vanish when the coupling is performed.

In TURBU, the connection to a 'more inner' subcomponent model is established by 'importing acceleration and speed variables' and 'exporting force and torque variables'. This allows for *not including* the 'inner' boundary dofs in the reduced order submodel. The reason for this is the following:

⇒ *The imported kinematic variables at the subcomponent entry point always provide the full rigid body motion of the subcomponent of which the reduced order model is derived.*

The exit point of the rotor blade profile submodel D_p is NOT connected to another submodel. This allows for leaving out *all* boundary DOFs from the reduced order submodel. However, the exit point of the tower subcomponent is connected to the nacelle subcomponent. Therefor the boundary dofs at the tower exit point are to be included in the reduced order model.

TURBU allows for switching on or off the flexibility of deformation orientations such as edgewise blade bending. It appeared that the model reduction procedure works well for all choices of deformability. The correspondence of the transfer functions before and after model reduction was pointed out to be decisive. This correspondence is a hard requirement, but necessary when the reduced order model is used for control design.

Equal transfer function behaviour implicitely guarantees equal eigenvalues. The correspondence of transfer functions required to include the quasi steady behaviour of the high-frequency modes in the subcomponent models D_p and S_t.

5 Control design

The state space model in fixed-frame coodinates by equation (7) is very feasible for control design. The three transformed pitch angles in the fixed frame represent actuation of (i) the aerodynamic torque and thrust force, (ii) the aerodynamic tilt moment, and (iii) the aerodynamic yaw moment. This also holds for corresponding transformed wind speed varations on the three rotor blades.

First, the servo behaviour of the pitch actuator is examined. Afterwards, the synthesis of different feedback structures is treated. Finally, closed loop transfer functions for the fixed-frame model are presented.

5.1 Pitch servo behaviour

Figure 6 shows the servo behaviour of pitch actuation with a collective and with a yaw orientation.

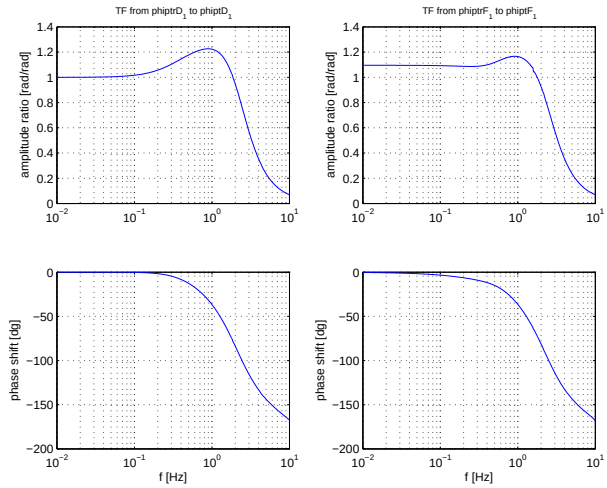

Figure 6: *Servo behaviour for collective (left) and yaw-oriented pitch actuation (right; tilt equal); amplitude ratio's between 'pitch angle output' and 'pitch angle reference' values (upper); phase lead angles of output relative to reference values (lower)*

The collective servo behaviour looks as expected: unit low-frequency gain and minor overshoot in the cut-off frequency of near 1Hz. However, the yaw-oriented servo behaviour differs. The steady-state gain (0-frequency) of 1.1 can be explained from the yaw orientation: the 0-frequency yaw-servo gain corresponds with the (collective-)servo gain in the 1p-frequency in the rotating frame of reference, viz. the 'rotating world in which the pitch servo actuator works'. The collective-servo gain near 0.3 Hz shows an amplitude ratio of 1.1,

which agrees with the quasi-steady yaw-servo gain of 1.1.

5.2 Feedback structures

Feedback structures were synthesized for a 3-bladed variable speed pitch controlled 3MW horizontal axis wind turbine. The control concepts that were realised with the feedback structures are:

- rotor speed reguluation by collective pitch;
- drive-train damping by generator torque;
- fore-aft tower damping by collective pitch;
- sidward tower damping by generator torque;
- 1p blade load reduction by cyclic pitch.

Lately, different approaches have been developed to provide applicable feedback structures. Approaches to basic speed regulation can be found in [11] and [26]. For fore-aft tower damping and drive-train damping is referred to [11] and [27]. Methods for the design of a blade load reduction algorithm by cyclic pitch control can be found in [28] and [29]. For basics on control theory see [30].

The synthesis procedure applied here is described in [31], except the drive-train damping is realised in accordance with the approach as proposed by Bossanyi in [11], in which the band-pass filter generator speed is fed back to the generator torque. The rotor speed regulation is based on scheduled PI-feedback from the rotor speed to the collective pitch angle angle setpoint.

The remaining feedback structures are the following:

- P-feedback of the band-pass filtered fore-aft tower top speed to the collective pitch angle setpoint for fore-aft tower damping;
- P-feedback of the band-pass filtered sideward tower top speed to the generator torque for sideward tower damping.
- I-feedback of the low- and band-pass filtered tilt and yaw component of the fixed-frame blade root moment coordinates to the tilt and yaw components of the fixed-frame pitch angle setpoints for 1p blade load reduction;

The second and third (fixed-frame) coordinate of the blade root moment output variables in the model formulation by equation (7) are proportional to the aerodynamic tilt and yaw torque. The regulation of the tilt and yaw torque corresponds with the reduction of the blade flap moments around the 1p-frequency. An important point of view is the approximate orthogonality of pitch control for the (i) aerodynamic torque and thrust, (ii) rotor yaw moment and (iii) rotor tilt moment.

The parameters for regulation of the yaw and tilt moment and of the rotor speed were determined by applying phase and gain margin constraints to the following design equations:

$$\begin{aligned}(J_\mathrm{r}+J_\mathrm{g})\cdot\Omega_\mathrm{gen}(t) &= 3\cdot k_{\mathrm{M_x}}\cdot\theta_{\mathrm{cm_1}}(t-\tau_{\mathrm{v_p}})\\ M_{\mathrm{cm_2}}(t) &= k_{\mathrm{M_z}}\cdot\theta_{\mathrm{cm_2}}(t-\tau_{\mathrm{v_p}})\\ M_{\mathrm{cm_3}}(t) &= k_{\mathrm{M_z}}\cdot\theta_{\mathrm{cm_3}}(t-\tau_{\mathrm{v_p}})\end{aligned} \tag{11}$$

The parameters $k_{\mathrm{M_x}}$ and $k_{\mathrm{M_z}}$ map a blade-specific pitch angle variation to a variation in the leadwise and flapwise blade root moment. These parameters are derived from power and thrust coefficient tables under the assumption of equal aerodynamic efficiency over the rotor radius. The inertia moments J_r and J_g pertain to the rotor and generator. The pitch-delay $\tau_{\mathrm{v_p}}$ is chosen such that it causes a phase delay that equals the expected phase delay from data processing and cyclic blade pitching; $\tau_{\mathrm{v_p}}$ was set to 0.14 s.

The parameters for damping enhancement of the tower and drive-train were derived from a desired damping rate associated with the design equations. The following design equations are allowed when suitable band pass filters are included:

$$\begin{aligned}&(\tfrac{J_\mathrm{r}\cdot J_\mathrm{g}}{J_\mathrm{r}+J_\mathrm{g}}\cdot\tfrac{\mathrm{d}^2}{\mathrm{dt}^2}+d_\mathrm{sh}\cdot\tfrac{\mathrm{d}}{\mathrm{dt}}+s_\mathrm{sh})(\gamma(t)) = \tfrac{J_\mathrm{r}}{J_\mathrm{r}+J_\mathrm{g}}\cdot\delta T_\mathrm{g}(t-\tau_{\mathrm{v_g}})\\ &(m_\mathrm{t}\cdot\tfrac{\mathrm{d}^2}{\mathrm{dt}^2}+d_\mathrm{t}\cdot\tfrac{\mathrm{d}}{\mathrm{dt}}+s_\mathrm{t})(x_\mathrm{sd}(t)) = \tfrac{3}{2H}\cdot\delta T_\mathrm{g}(t-\tau_{\mathrm{v_g}})\\ &(m_\mathrm{t}\cdot\tfrac{\mathrm{d}^2}{\mathrm{dt}^2}+d_\mathrm{t}^*\cdot\tfrac{\mathrm{d}}{\mathrm{dt}}+s_\mathrm{t})(x_\mathrm{fa}(t)) = 3k_{\mathrm{F_x}}\cdot\theta_{\mathrm{cm_1}}(t-\tau_{\mathrm{v_p}})\\ &\qquad\text{with}\;\; d_\mathrm{t}^* = d_\mathrm{t}+3h_{\mathrm{F_x}}-\tfrac{81Rb}{32H^2}\cdot h_{\mathrm{M_z}}\end{aligned} \tag{12}$$

The parameters s_sh and d_sh, together with the inertia moment $J_\mathrm{r}\cdot J_\mathrm{g}/(J_\mathrm{r}+J_\mathrm{g})$, model the behaviour of the first collective leadlag rotor/drive-train mode. The torque-delay $\tau_{\mathrm{v_p}}$ amounts to 0.045 seconds, an estimation for the data processing time and transient behaviour of the generator torque servo.

The parameters $k_{\mathrm{F_x}}$ and $h_{\mathrm{F_x}}$ map a blade-specific pitch angle and blade-uniform wind speed variation to a variation in the axial force on the blade root. The parameters m_t, d_t and s_t model the *translation* behaviour of the first bending mode of the tower, which is assumed to be equal in foreaft and sideward direction. The effect on the fore-aft

translation by the tilt *rotation* of the tower top is modelled via the coefficient $-81R\mathrm{b}/(32H^2)$, with $R\mathrm{b}$ and H the rotor radius and tower height. The associated term in the fore-aft bending equation represents a force that is derived from the estimated tilt moment caused by the tilt rotation.

The choice of filters is crucial in order to allow for the 'scalar' classic PID-approach. The band-pass filters are designed such that the phase shift of filter and loop delay together amounts to zero in the respective natural frequencies.

5.3 Closed loop transfer functions

Figure 7 shows the sensitivity of the rotor speed and tower bottom fore-aft moment to wind speed variations with a collective and tilt-wise orientation. The dashed blue lines represent the open loop behaviour while the solid red lines appear when the basic controller is linked to the wind turbine. It can be observed that the rotor speed

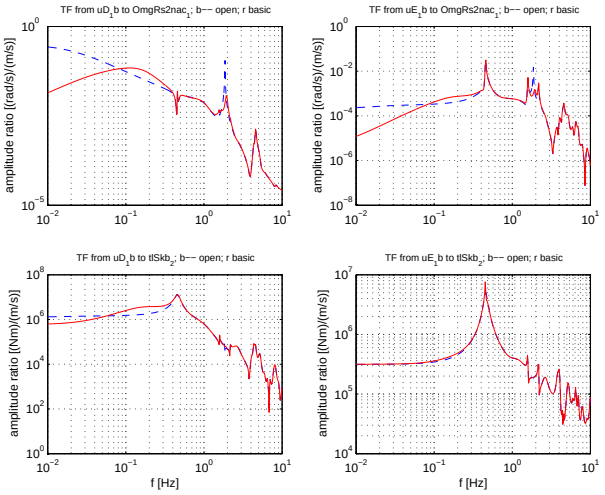

Figure 7: *Sensitivity of rotor speed (upper) and tower bottom fore-aft moment (lower) to collective (left) and tilt-oriented (right) wind speed variations of the wind turbine without (blue dash) and with (red solid) basic control*

variations from the turbulence are reduced by the controller in frequencies up to 0.08 Hz. This also holds, in less sense, for the fore-aft moment. However, between 0.1 and 0.4 Hz the closed loop behaviour is slightly worse than the open loop behaviour. Since the 'energy' of the turbulence is largely concentrated in frequencies below 0.1 Hz, the overall behaviour is (of course) expected to be improved, especially as concerns the rotor speed behaviour.

It is also clear from Figure 7 that the drive-train vibrations are significantly reduced: the peak in the amplitude ratio just below 2 Hz is reduced by a factor 10 approximately.

The closed loop configuration with cyclic pitch and basic control included was extended with the add-ons for fore-aft and sideward tower damping. This yielded the overall closed loop model in 18 m/s.

Figure 8 shows the sensitivity of the rotor speed and tower bottom fore-aft moment to wind speed variations with a collective and tilt-wise orientation.

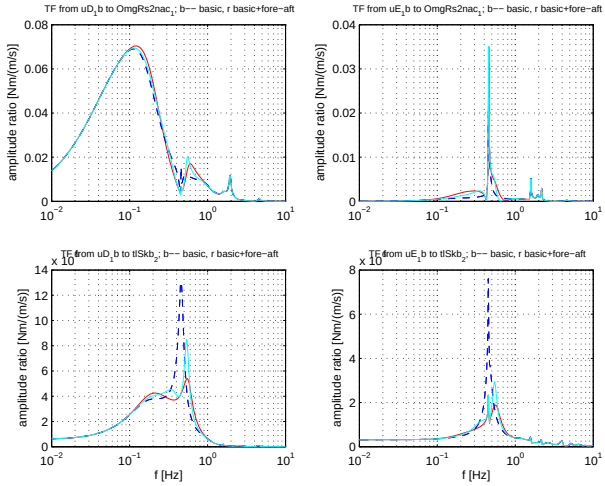

Figure 8: *Sensitivity of rotor speed (upper) and tower bottom fore-aft moment (lower) to collective (left) and tilt-oriented (right) wind speed variations in case of basic control (blue dash) and with add-on for fore-aft tower damping from collective pitch (red solid)*

The dahsed blue lines represent the behaviour with the basic controller while the solid red [black] lines appear when collective pitch control for enhanced fore-aft damping is added. The solid cyan [grey] lines pertain to the 'fore-aft damping add-on' with other parameters:

- the 'red' [black] enhanced fore-aft damping behaviour is achieved with a filter with with a pass band between 25% and 400% of the natural first tower fore-aft frequency;
- the 'cyan' [grey] enhanced fore-aft damping behaviour is achieved with a filter with with a pass band between 50% and 200% of the natural first tower fore-aft frequency.

It appears that the wide '25% - 400%' filter yields both a more wide and a less high peak while the moderate '50% - 200%' filter yields a more narrow but less high peak. Since the more narrow peak

for the moderate filter is *lower* than the original wider peak the use of the moderate filter is yet expected to effectively reduce the fore-aft loading. In simple analysis on 'second order dynamics' the occurrence of more narrow and yet lower peak is not expected. However, a full dynamic model allows for this paradoxal property; it follows from the interaction of deformation modes.

Analysis with doubled feedback gain showed less damping enhancement but still stable closed loop behaviour.

Figure 9 shows the sensitivity of the rotor speed and tower bottom sideward moment to wind speed variations with a collective and yaw-wise orientation.

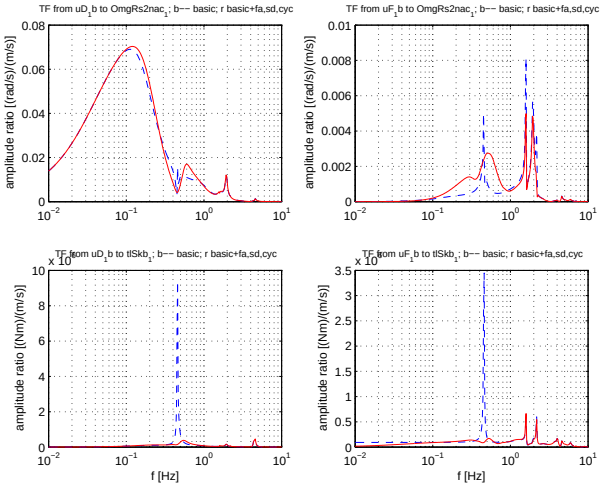

Figure 9: *Sensitivity of rotor speed (upper) and tower bottom sideward moment (lower) to collective (left) and yaw-oriented (right) wind speed variations in case of basic control (blue dash) and with all add-ons included (red solid)*

The dashed blue lines represent the behaviour with the basic controller while the solid red lines appear when generator torque control for enhanced sideward damping is added. The applied pass band ranges from 50% to 200% of the first natural sideward tower frequency.

The sensitivity of the tilt and yaw moment to tilt- and yaw-oriented wind speed variations is depicted in Figure 10.

The dashed blue [black] lines represent the behaviour with basic control only, while the solid red [black] lines pertain to the behaviour with cyclic pitch control included. The gains in the yaw and tilt moment feedback loops were reduced to 50% of the allowed values. Analysis with doubled feedback gains, the *actual design values*, showed steeper decay of the amplitde ratios frequency be-

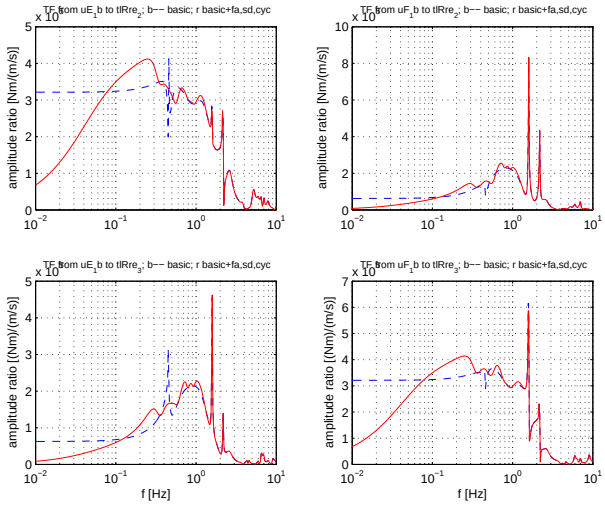

Figure 10: *Sensitivity of tilt moment (upper) and yaw moment (lower) in the rotor centre to tilt- (left) and and yaw-oriented (right) wind speed variations in case of basic control (blue dash) and with all add-ons included (red)*

low 0.1 Hz but the disturbance *amplification*, instead of desired reduction, strongly increases beyond ca 0.1 Hz. This would lead to a strong *enlargment* of the turbulence induced loads in frequency just below 1p - 0.1Hz and just aboe 1p + 0.1Hz. Instable closed loop behaviour is observed at 4.5 times the applied feedback gains.

6 Time domain simulation

Time domain simulations were performed with the aeroelastic simulation code PHATAS [16] in 18 m/s at 17% turbulence with an exponential shear coefficient of 0.20. The wind field was obtained with the ECN program SWIFT [32], [33]. All feedback structures that were analysed in the previous section were linked to PHATAS via a DLL derived from a MATLAB-implementation via the MATLAB-C-compiler.

Figure 11 shows the auto power spectra of the tower-bottom fore-aft moment, tower-bottom sideward moment, blade root flap moment and tilt moment in the rotor centre in four boxes. Each box contains the power spectrum for the case of basic control (null) only, and for the case with all feedback structures included.

The merits of the feedback strcutures for load reduction are clearly observable from the reduced spectral peaks

- in and around the tower natural frequency

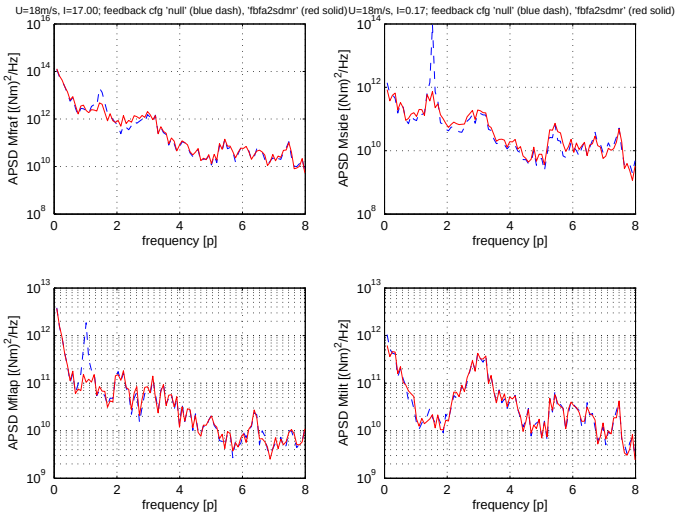

Figure 11: *Power spectrum of bottom fore-aft moment (upper left), bottom sideward moment (upper right), blade root flap moment (lower left) and tilt moment (lower right) for basic controller (dash) and extension with all add-ons in 18m/s (solid)*

for the tower bottom moments;

- in and around the 1p-frequency for the blade root moment

Only (very) low frequent reduction is observed for the tilt (and yaw) moment. Note that the average tilt and yaw loading are almost nihilated; this is not observable in figure 11 because the average values were not included in the power spectra.

Within the STABCON project, statistical representative simulations were performed for different turbulence levels, mean wind speeds and exponential shear factors. Design guidelines for aeroelastic control were deduced from the results and are being published [35]. The potential of the load reducing controllers has been derived from the '1p-equivalent fatigue loads'. The controller from this paper showed a typical reduction potential of

- 10% to 30% for the rotor blade fatigue loading
- 4% to 6% for the tower fatigue loading.

Under extreme turbulent or shear conditions the reduction levels deviate from these values. In stronger shear conditions the potential increases, while it decreases at stronger turbulence. It is expected that more sophisticated control methods will result in higher reduction levels. Especially, the reduction of (i) low-frequent tower and blade loads, in the time-scale of rotor uniform turbulence and (ii) blade loads around 2p, and thus tilt- and yaw-loading around 3p, still offers large possibilities for reduction of the component costs. Scoping results of the latter option were already reported in [29]. Distributed blade actuation such as variable trailing edge geometry may play an important role in further load reduction by control.

7 Conclusion

The ECN computer code TURBU generates an integrated linearised aerohydro-elastic model with control, wave and wind inputs for 3-bladed wind turbines. It also calculates the equilibrium state. As a matter of fact TURBU extends a regular advanced linear aeroelastic stability tool with the capability to transfer function analysis and linear time-domain simulation in both open and closed loop conditions.

Closed loop transfer function analysis with TURBU proves that feedback loops for enhanced sideward and fore-aft tower damping and reduced blade loads around 1p can be derived well from simple design equations. Only some filters related to collective pitch control had to be retuned.

The validity of closed loop transfer function predictions has been proved in non-linear aeroelastic time-domain simulations. These simulations showed significant load reduction and good closed loop stabilty. The fatigue loads in full load operation were reduced by 10% to 30% for the rotor blades and 4% to 6% for the tower. The rate of achievable blade load reduction around 1p depends on the ratio between shear and turbulence influences. The larger the shear influence, the higher the achievable reduction level is. Further significant load reduction is expected from distributed blade actuation, both in the very low frequency range and in the frequency range around 2p.

A TURBU model includes bending and torsion deformation of the tower and rotor blades, shear centre offset, (unsteady) aerodynamic conversion, wake dynamics, pitch servo dynamics and hydrodynamic conversion. The linearisation is centered around average conditions that include prebend and twist of the rotor blades, average deformation and average induction (BEM).

The inclusion of model reduction schemes for the blade and tower submodels makes TURBU computationally very efficient. Its modular structure facilitates convenient implementation of extensions in future. These may e.g. pertain to distributed blade actuation, like variable trailing edge geometry as scoped by Buhl e.a. [34], or to include a second pitch actuator in the mid-span

location of the rotor blades. The modular structure also allows to use a separately derived model for a deviating support structure, such as a lattice tower or even a floating platform.

TURBU is programmed in the MATLAB programming language [4] and is available for use by third parties. The program input agrees with that required by non-linear aeroelastic time domain simulation codes like PHATAS. The only deviation concerns 3D-correction of the lift polars, which has to be performed beforehand.

On a 1.6 GHz Pentium Mobile processor:

- the creation of an integrated dynamic model including equilibrium assessment for one working point amounts to 12 s;
- model reduction reduces the computation time for bode diagrams from tens of seconds to fractions of a second.

Acknowledgement

Mr. Herman Snel, Koert Lindenburg and Danny Winkelaar (all ECN) are acknowledged for the proposed modelling procedure for the effect of non-coinciding shear and elastic centres. In addition Koert and Danny are acknowledged for the initiating actions with respect to the applied method of model reduction. Danny and Mr. Johan Peeringa (ECN) are acknowledged for providing wind files via the ECN program SWIFT and for the facilitation of the non-linear time-domain simulation ECN program PHATAS.

Mr. Eric van der Hooft and Pieter Schaak (both ECN) and Mr. Ben Hendriks, Theo de Lange and Luc Rademakers of the management of the ECN Wind Energy group are acknowledged for continuous support during the development of TURBU.

SenterNovem and the Dutch Ministry of Economic Affairs are acknowlegded for supporting the development, the use and the tailoring to control design of TURBU under grants 2020-01-12-10-001 and EOSLT02013 in the projects "TURBUOffshore, Implementation" and "Sustainable Control, a new Approach to Operate Wind Turbines (SUSCON)" in respectively the TWIN- and EOS research programmes.

The EU and SenterNovem are acknowledged for supporing the verification, the use and the tailoring to aero-ealastic analysis of TURBU under grants ENK5-CT-2002-00627 and 2020-02-11-10-007 in the project "Aeroelastic Stability and Control of Wind turbines (STABCON)". The complete STABCON project group is acknowledged for very pleasant and inspiring cooperation.

References

[1] J.B. Dragt; *Load fluctuations and response of rotor systems in turbulent wind fields*, Extern report ECN-172, ECN Windenergie, 1985, Petten, the Netherlands

[2] J.B. Dragt; *Atmospheric turbulence characteristics in the rotating frame of reference of a WECS rotor*, in *Proceedings EWEC 1990*, pp 274-278, Madrid, Spain

[3] T.G. van Engelen, J. van der Tempel; *Frequency Domain Load Calculation for Offshore Wind Turbines (TURBU Offshore)*, in *Proceedings of EWEC 2004*, London, UK

[4] The Mathworks Inc.; *MATLAB The Language of Technical Computing*, 7$^{\text{th}}$ edition, Natck, MA, USA, www.matlab.com

[5] T.J. McCoy; *Wind Turbine ADAMS Model Linearization for Control Design Including Rotational and Aerodynamic Effects* in Proceedings of special topic conference on 'the Science of Making Torque from Wind', pg 498-508, April 2004, Delft, the Netherlands

[7] M.A. Crisfield; *A Consistent Co-rotational Formulation for Non-linear Three-dimensional Beam Elements*, in *Computational Methods Applied Mechanical Engeneering, 81:131-150*, 1990

[8] J.M. Battini, *Co-rotational Beam Elmeents in Instability Problems*, PhD-thesis, January 2002, Royal Institute of Technology, Dept. of Mechnics, Stockholm, Sweden.

[9] R.L. Bielawa, *Rotary Wing Structural Dynamics and Aeroelasticity*, American Institute of Aeronautics and Astronautics, Inc., 1995, 370 L'Enfant Promenade, SW, Washington, DC 20024-2518, USA

[10] T.R. Kane, D.A. Levinson; *Dynamics, Theory and Applications*, McGraw-Hill series in Mechanical Engineering, 1985

[11] T. Burton, D. Shape, N. Jenkins, E.A. Bossanyi; *Wind Energy Handbook*, 2001, John Wiley & Sons Ltd, Chichester, West Sussex, UK

[12] H. Snel; *Heuristic Modelling of Dynamic Stall Characteristics*, in *Proceedings EWEC 1997, pg 429-433*, Dublin Castle, Ireland

[13] J.F. Wilson; *Dynamics of Offshore Structures*, John Wiley & Sons, 1984

[14] H. Snel, J.G. Schepers; *Joint Investigation of Dynamic Inflow Effects and Implementation of*

an Engineering Method. Technical Report ECN-C-94-107, April 1985, ECN Wind Energy, Petten, the Netherlands.

[15] H. Snel, J.G. Schepers; *Engineering Models for Dynamic Inflow Phenomena*, pg 267-281, in Journal of Wind Engineering and Industrial Aerodynamics, Elsevier Science Publ. Amsterdam, 1992.

[16] C. Lindenbur, J.G. Schepers; *PHATAS-IV, Aeroelastic Modelling*, Technical Report ECN-C–00–27, 2000, ECN Wind Energy, Petten, the Netherlands

[17] J.G. Schepers, *An Engineering Model for Yawed Conditions, Developed on the Basis of Wind Tunnel Measurements*, Technical Report ECN-RX--98-057, Netherlands Energy Research Foundation ECN, Petten, The Netherlands, 1999.

[18] R.E. Wilson, *Aerodynamic potpourri*, in *Proceedings of the first DOE/NASA Wind Turbine Dynamics Workshop*, State University, Cleveland, Ohio, 1981; also published as NASA CP 2185.

[19] T.G. van Engelen, L.D. Hofland, J.H. Vugts; *TURBU Offshore; Model Description (in Dutch)*, Technical Report ECN-C–02-73, November 2002, ECN Wind Energy, Petten, the Netherlands

[20] T.G. van Engelen, H. Braam; *TURBU Offshore; Implementation*, Technical Report ECN-C–04-79, September 2004, ECN Wind Energy, Petten, the Netherlands

[21] R.P. Coleman, A.M. Feingold, *Theory of Self-Excited Mechanical Oscillations of Helicopter Rotors with Hinged Blades*, NASA TN 3844, NASA, Februari 1957.

[22] W.C. Hurty; *Dynamic Analysis of Structural Systems by Component Mode Synthesis*, Rept. 32-530, Jet Propulsion Lab., Pasadena, California, December 1964.

[23] W.C. Hurty; *Dynamic Analysis of Structural Systems Using Component Modes*, in *AIAA Journal*, Vol. 3(4):678–685, 1965.

[24] R.R. Craig Jr, M.C.C. Bampton; *Coupling of Substructures for Dynamic Analyses*, in *AIAA Journal*, Vol. 6(7):1313–1319, 1968.

[25] M.H. Hansen, *Aeroelastic Stability Analysis of Wind Turbines Using an Eigenvalue Approach*, in *Proceedings EWEC 2003*, Madrid, Spain

[26] T.G. van Engelen, E.L. van der Hooft, P. Schaak, *Development of Wind Turbine Control Algorithms for Industrial Usage*; in *Proceedings EWEC 2001*, Copenhagen, Danmark.

[27] E.A. Bossanyi; *Wind Turbine Control for Load Reduction*, in *Wind Energy, No. 6, pg 229-224*, 2003

[28] E.A. Bossanyi; *Developments in Individual Blade Pitch Control*, in Proceedings of special topic conference on 'the Science of Making Torque from Wind', pg 486-497, April 2004, Delft, the Netherlands

[29] T.G. van Engelen; *Design Model and Load Reduction Assessment for Multi-rotational Mode Individual Pitch Control (Higher Harmonics Control)* in *Proceedings of EWEC 2006*, Athens, Greece

[30] K.J. Astrom, B. Wittenmark; *Computer controlled systems: theory and design*, Prentice-Hall , Inc., EngleWood Cliffs, New Jersey 07632, 1984

[31] , T.G. van Engelen, H. Markou, T. Buhl, B. Marrant; *Morpholocial Study of Aeroelastic Control Concepts for Wind Turbines, STABCON Task-7 Report*; EU contract ENK5-CT-2002-00627, ECN-E-06-056, ECN Wind Energy, December, 2006, Petten, the Netherlands

[32] D. Winkelaar; *SWIFT, Program for Three-Dimensional Wind Simulation, Part 1: Model Description and Program Verification*, Technical Report ECN-R--92-013, December 1992, ECN Wind Energy, Petten, the Netherlands

[33] D. Winkelaar; *SWIFT, Ontwikkeling en validatie van een stochastisch windbelastingsmodel. Deel 1. Windmodellering*, Technical Report ECN-C–06-096, December 1996, ECN Wind Energy, Petten, the Netherlands

[34] T. Buhl, T. M. Gaunaa and C. Bak; *Potential load reduction using airfiols with variable trailing edge geometry.* In *Journal of Solar Energy Engineering, 127(4):503-516*, November 2005.

[35] T. Buhl, K. Thomsen, H. Markou (editors); *Design Guidelines for Integrated Aeroelastic Control of Wind Turbines, STABCON Task-12 Report.* EU contract ENK5-CT-2002-00627, <in preparation>, Riso National Laboratoy, Roskilde, Denmark, 2007

A Model equations

This appendix aims at providing a complete explantion of the underlying model equations that are used in the component models. The four sections address the model equations for the rotor blades, drive-train, support structure and the wake.

A.1 Rotor blade equations

A.1.1 Flange D_f and profile & structure D_p

The structural dynamic behaviour of the rotor blade is modelled under the assumption of massless elastic beam elements and concentrated point masses to which moments of inertia are attributed. In figure 12 five of such beam elements of length S are distinguished.

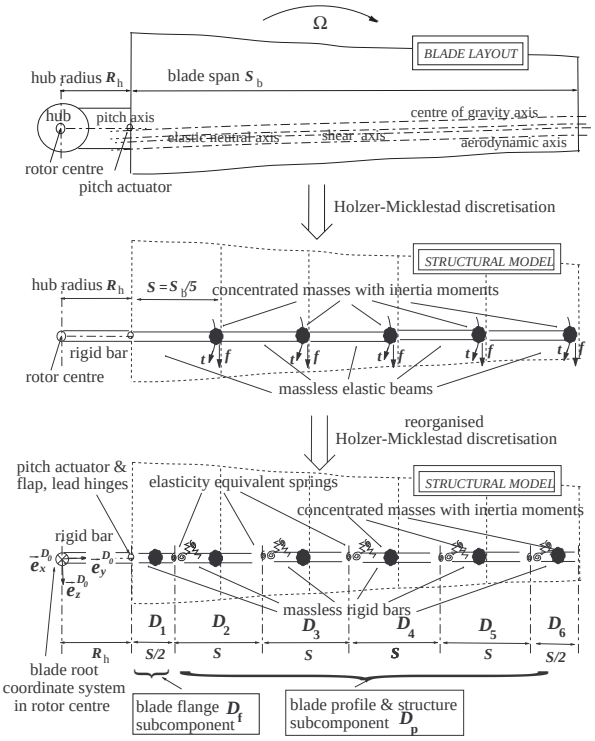

Figure 12: *Structural blade model*

Consider the bending deformation at the end of a beam element from concentrated force and torque loads f and t along unit vectors $\underline{e}_z^{D0}$ and $\underline{e}_x^{D0}$ in that location for invariant stiffness EI over an element (beam bending equivalence). Exactly the same deformation is obtained with a concentrated angular and linear spring in the mid-span location with stiffness EI/S and $12EI/S^2$ respectively. In our model, the massless elastic beams are replaced by these springs and rigid bars. The *effective* bending stiffness EI is based on the maintenance of similar rotation per moment characteristics (the bending moment is assumed almost constant along the beam element). It then holds

$$EI = S \;/\; \left(\int_{s_0}^{s_\mathrm{e}} \frac{s}{EI(s)} \cdot \mathrm{d}s \right) \qquad (13)$$

Two orthogonal bending spring pairs are located in the mid-span location of each of the five beam elements in order two model blade bending in two directions. Also, springs are added for the torsional deformation.

As so far, the Holzer-Myklestad method as described by Bielawa in [9] is followed, except a slight reallocation of mass and the added torsion springs. Figure 12 shows that the rotor blade model consists of the 5 elements $D_2 \ldots D_6$ that set up the blade profile & structure D_p and an additional element D_1 that is used for for the flange D_f. The flange element D_1 transduces the rigid body motion from the end of the blade root to the entry point of the first blade profile & structure element D_2. The flange element D_1 allows for motion relative to the blade root, via pitching and flap and leadwise hinges. For the sake of equally structured equations of motions for all elements, the blade mass beteen 0 and $\frac{1}{2}S$ of the blade span S_b is allocated to D_1. The inertia properties of elements $S_2 \ldots S_5$ and S_6 are derived from integrals over span intervals $\{\frac{1}{2}S, \frac{3}{2}S\} \ldots \{\frac{7}{2}S, \frac{9}{2}S\}$ and $\{\frac{9}{2}S, S_\mathrm{b}\}$.

Note that the mid-span locations of the *model* elements $D_2 \ldots D_5$ correspond with the end points of the first four *beam* elements according to Holzer & Myklestad. In order to maintain as much as possible the principle of 'beam bending equivalence', the spanwise distributed aerodynamic loads are mapped to concentrated loads in:

- mid-span locations of elements $D_2 \ldots D_5$;
- end point of element D_6;
- entry point of element D_1.

The mapping procedure is based on equal deformation in the end points of massless elastic beam elements, just as mentioned above for the dimensioning of the springs.

Before the model equations can be derived, the structural model is cast into a co-rotational formulation in such a way that the *angular* bending springs are located on the elastic axis. An exception concerns element D_1 and those that are preceeded by elements for which explictely out of plane and in-plane configuration angles are defined (coning angle(s), δ_3-angle(s)). In D_1 the location of angular springs coincides with the pitch axis while in the latter elements the location of these springs follows from the configuration angles. This allows for coning, flap and leadwise skewness, prebend and the inclusion of the averaged deformed state in the equations of motion.

Figure 13 shows in the upper part the configuration of model element D_3 via the spanwise elastic (y-)axis and the neutral bending axes for edge and flatwise bending (x- and z-axis). The edge- and flatwise orientation are obtained by 'nose-up' ro-

tation over the structural pitch angle relative to the in-plane and out of plane orientation (lead- and flapwise). The local coordinate system $\underline{e}_{1,2,3}^{D_3}$ coincides with the 'elastic' x-, y- and z-axis of D_3 and is used for the formulation of the equations of motion in the entry point $D_3^{\ominus}$.

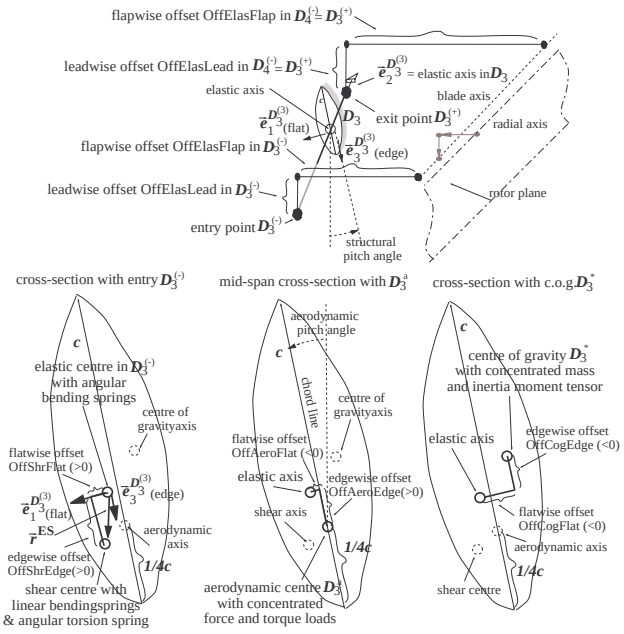

Figure 13: *Configuration and center points of 3rd blade model element*

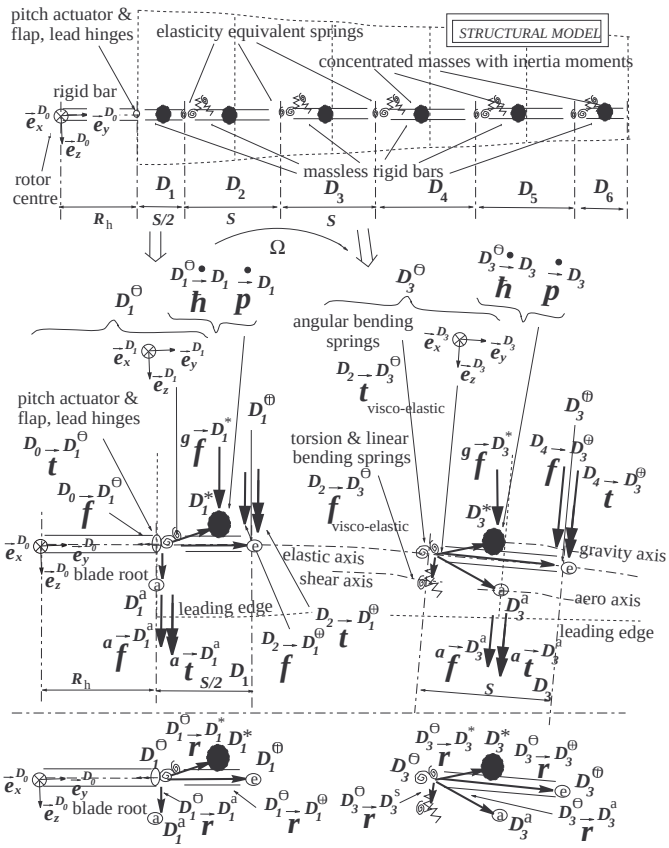

Figure 14: *Equation of motion governing vector variables for 1st and 3rd blade model element*

The lower part of the figure shows (i) the shear centre in the cross section with the entry point $D_3^{\ominus}$, (ii) the mid-span cross section with the aerodynamic conversion point D_3^{a} for the concentrated aerodynamic force and torque loads and (iii) the cross section in which the centre of gravitiy D_3^{*} is located. The chord line is 'nose-up positive' rotated over the aerodynamic pitch angle relative to the in-plane orientation. The effect on deformation through the shear axis offset from the elastic axis is modelled as follows: the *linear* bending springs and the *torsion* spring are moved to the shear centre over place vector $\underline{r}^{\mathrm{ES}}$ while the *angular* bending springs remain located in the elastic centre. Elements $D_2 \ldots D_6$ are all treated in the same way.

The equations of motion for the blade elements are derived by Newton's law related to the rate of change in the linear impulse and in the angular impulse relative to the entry point of each element. Figure 14 shows the relevant load, place and impulse vectors for the blade flange element D_1 and the profile & structure element D_3.

The coordinate system independent vector expressions for the equations of motion of element D_3 are the following:

$$
\begin{aligned}
{}^{D_3^{\ominus}}\dot{\vec{\hbar}}^{D_3} &= {}^{\mathrm{RS}}\vec{t}^{\,D_3^{\ominus}} + {}^{D_4}\vec{t}^{\,D_3^{\oplus}} + {}^{D_3^{\ominus}}\vec{r}^{\,D_3^{\oplus}} \times {}^{D_4}\vec{f}^{\,D_3^{\oplus}} + \\
&\qquad {}^{\mathrm{a}}\vec{t}^{\,D_3^{\mathrm{a}}} + {}^{D_3^{\ominus}}\vec{r}^{\,D_3^{\mathrm{a}}} \times {}^{\mathrm{a}}\vec{f}^{\,D_3^{\mathrm{a}}} + {}^{D_3^{\ominus}}\vec{r}^{\,D_3^{*}} \times {}^{\mathrm{g}}\vec{f}^{\,D_3^{*}} \\
\dot{\vec{p}}^{D_3} &= {}^{\mathrm{RS}}\vec{f}^{\,D_3^{\ominus}} + {}^{D_4}\vec{f}^{\,D_3^{\oplus}} + {}^{\mathrm{a}}\vec{f}^{\,D_3^{\mathrm{a}}} + {}^{\mathrm{g}}\vec{f}^{\,D_3^{*}}
\end{aligned}
\tag{14}
$$

The responsive loads ${}^{\mathrm{RS}}\vec{t}^{\,D_3^{\ominus}}$ and ${}^{\mathrm{RS}}\vec{f}^{\,D_3^{\ominus}}$ are visco-elastic loads; in the blade flange, the torque component along the y-axis usually results from the pitch actuator.

What is referred to as the rate of change of angular impulse actually is the *biased* angular impulse ($\hbar$ is used instead of h), which excludes the term that is set up by the linear acceleration of the reference point $D_3^{\ominus}$. The summed biased angular impulse change relative to $D_3^{\ominus}$ equals the torque load in $D_3^{\ominus}$ (see discussion in §5.1.3 of [19]). For the angular and linear impulse of the element D_3

holds (no coordinate system reference):

$$
\begin{aligned}
{}^{D_3}_{\ominus}\dot{\vec{h}}^{D_3} &= {}^{D_3}_{\ominus}\vec{r}^{D_3^*} \times \dot{\vec{p}}^{D_3} + \boldsymbol{I}^{D_3} \bullet \vec{\alpha}^{D_3} + \vec{\omega}^{D_3} \times \boldsymbol{I}^{D_3} \bullet \vec{\omega}^{D_3} \\
\dot{\vec{p}}^{D_3} &= m^{D_3} \vec{a}^{D_3^*}
\end{aligned}
\tag{15}
$$

In this expression is $\boldsymbol{I}$ the *central inertia dyadic* as defined by Kane and Levinson [10]. When the equation is expressed as a normal vector differential equation in coordinates along a (local) coordinate system, then $\boldsymbol{I}$ gets the meaning of the so called inertia tensor, a 3×3-matrix with the principal moments of inertia on the diagonal.

The structural velocity and acceleration contribute to both the impulse and the load vectors in equation (14). These kinematic variables are expressed in coordinates along the local coordinate systems of the elements, such as $\vec{e}^{\,D_3}_{(x,y,z)}$ and $\vec{e}^{\,D_1}_{(x,y,z)}$ in figure 14, in accordance with the method proposed by Kane and Levinson [10].

Before we continue with the treatment of the kinematic variables, it is clarified how the DOFs are included in the model description. A complete treatment of the DOFs is given in App. B of [20].

Degrees of freedom (DOFs)

The angular and linear DOFs are modelled as incremental rotations $\phi^{D_m}_{(1,2,3)}$ and translations $\rho^{D}_{(1,2)}$ in the entry point of an element D_m (axial translation not taken into account). The bottom-up ranking of the rotations in the *flange* element is *flap-pitch-edge*, so alng the local z-,y- and x-axis; and in the *blade structure* elements *pitch-flat-edge*, so along the local y-,z- and x-axis. The corresponding bottom-up ranked translations are along the x-, z-axis and z-, x-axis respectively.

The rotation ranking is chosen such that blade coning and δ_3 setting can be configured via the average values $\bar{\phi}_1^{D_1}$ and $\bar{\phi}_3^{D_1}$; the average pitch angle is carried through via $-\bar{\phi}_2^{D_1}$. Further, prebend and average blade bending are carried through via average rotations $\bar{\phi}_2^{D_{2\ldots N}}$ and $\bar{\phi}_3^{D_{2\ldots N}}$ while structural pitch and average blade torsion appear via $\bar{\phi}_2^{D_{2\ldots N}}$.

The angular DOFs on an element make the orientation of the coordinate system on that element differ from that on the foregoing element. The place vectors as depicted in figure 14 have invariant coordinates along the local coordinate systems.

Kinematics rotor blades

In order to facilitate the *modular* and *linear* approach of TURBU, in which the average deformation state is taken into account, a kinematic variable of an element is expressed:

- as a function of (i) the DOFs *within* the subcomponent of that element and (ii) the kinematic variables *at the end* of the *foregoing* subcomponent; the blade flange is foregoing to the blade profile&structure, the rotor shaft & hub is foregoing to the blade flange, etc.

- as a function with *linear* dependency on the *variations* of the DOFs and foregoing kinematic variables, in which the *average* values of the DOFS and the average rotor speed $\bar{\Omega}$ act as parameters of that function.

For example, the translation (=linear) velocity $\vec{v}^{\,D_3^{\mathrm{a}}}$ of the aerodynamic conversion point D_3^{a} is expressed in the linear and angular velocity at the exit point of the flange ($D_1^{\oplus}$) and the angular and linear DOFs in the entry points of elements D_2 and D_3. The coordinates of $\vec{v}^{\,D_3^{\mathrm{a}}}$ along $\vec{e}^{\,D_k}$ are obtained by:

$$
\begin{aligned}
\underline{v}^{D_3^{\mathrm{a}}} \;=\; & \bar{\underline{v}}^{D_3^{\mathrm{a}}} + \frac{\partial \underline{v}^{D_3^{\mathrm{a}}}}{\partial \underline{v}^{D^{\oplus}_{\mathrm{FF}}}} \cdot \delta \underline{v}^{D^{\oplus}_{\mathrm{FF}}} + \frac{\partial \underline{v}^{D_3^{\mathrm{a}}}}{\partial \underline{\omega}^{D^{\oplus}_{\mathrm{FF}}}} \cdot \delta \underline{\omega}^{D^{\oplus}_{\mathrm{FF}}} + \\
& \frac{\partial \underline{v}^{D_3^{\mathrm{a}}}}{\partial \underline{\phi}^{D}} \cdot \delta \underline{\phi}^{D} + \frac{\partial \underline{v}^{D_3^{\mathrm{a}}}}{\partial \underline{\dot{\varphi}}^{D}} \cdot \underline{\dot{\varphi}}^{D} + \frac{\partial \underline{v}^{D_3^{\mathrm{a}}}}{\partial \underline{\dot{\varrho}}^{D}} \cdot \underline{\dot{\varrho}}^{D}
\end{aligned}
\tag{16}
$$

For the average velocity $\bar{\underline{v}}^{D_3^{\mathrm{a}}}$ holds:

$$
\begin{aligned}
\bar{\underline{v}}^{D_3^{\mathrm{a}}} \;=\; & {}^{D_3}\bar{\Phi}^{D_1} \cdot \bar{\underline{v}}^{D_1^{\oplus}} + \\
& \Big(\sum_{m=2}^{3} {}^{D_3}\bar{\Phi}^{D_m} \cdot \mathrm{J}^{3}_{v=1}\big({}^{D_m}\bar{\Phi}^{D_1}_{v} \times {}^{D_m^{\ominus}}\underline{r}^{D^{\oplus|\mathrm{a}}_{m|3}}\big)\Big) \cdot \bar{\underline{\omega}}^{D_1}
\end{aligned}
\tag{17}
$$

The coordinates of the average velocity vector $\bar{\underline{v}}^{D_1^{\oplus}}$ at the flange-exit are mapped from the flange's coordinate system to that of element D_3 via ${}^{D_3}\bar{\Phi}^{D_1}$. This mapping includes the transformation over the average angular DOF-values of elements D_2 and D_3:

$$
\begin{aligned}
{}^{D_3}\bar{\Phi}^{D_1} \;=\; & {}^{D_3}\bar{\Phi}^{D_2} \cdot {}^{D_2}\bar{\Phi}^{D_1}\ , \ \text{with } (m = 2, 3): \\
& {}^{D_m}\bar{\Phi}^{D_{m-1}} = \Phi_{\mathrm{x}}(\bar{\phi}_3^{D_m}) \cdot \Phi_{\mathrm{z}}(\bar{\phi}_2^{D_m}) \cdot \Phi_{\mathrm{y}}(\bar{\phi}_1^{D_m})
\end{aligned}
\tag{18}
$$

For the incremental transformation matrix $\Phi_{\mathrm{z}}(\bar{\phi})$ holds (similar for $\Phi_{\mathrm{x}}(\bar{\phi})$ and $\Phi_{\mathrm{y}}(\bar{\phi})$):

$$
\Phi_{\mathrm{z}}(\bar{\phi}) = \begin{pmatrix} \cos\bar{\phi} & \sin\bar{\phi} & 0 \\ -\sin\bar{\phi} & \cos\bar{\phi} & 0 \\ 0 & 0 & 1 \end{pmatrix} \tag{19}
$$

The place vector ${}^{D^{\ominus}_m}\vec{r}^{\,D^{\oplus|\mathrm{a}}_{m|3}}$ runs to the exit point if $m < 3$ and to the aerodynamic conversion point if $m = 3$.

The expression $\mathrm{J}^{3}_{v=1}(.)$ implies that the results of the 3 vector products are put next to each other from left to right for $v = 1, 2, 3$.

For the sensitivity functions $\partial \underline{v}^{D_3^{\mathrm{a}}}/\partial \underline{v}^{D_{\mathrm{FF}}^{\oplus}}$ and $\partial \underline{v}^{D_3^{\mathrm{a}}}/\partial \underline{\omega}^{D_{\mathrm{FF}}^{\oplus}}$ holds:

$$\begin{aligned}
\frac{\partial \underline{v}^{D_3^*}}{\partial \underline{v}^{D_{\mathrm{FF}}^{\oplus}}} &= {}^{D_3}\bar{\Phi}^{D_1} \\
\frac{\partial \underline{v}^{D_3^*}}{\partial \underline{\omega}^{D_{\mathrm{FF}}}} &= \sum_{m=2}^{3} {}^{D_3}\bar{\Phi}^{D_m} \cdot \mathrm{J}_{v=1}^{3}({}^{D_m}\bar{\Phi}_v^{D_1} \times {}^{D_m^{\ominus}}\underline{r}^{D_{m|3}^{\oplus|\mathrm{a}}})
\end{aligned} \tag{20}$$

In order to be able to use a generic scheme for the derivation of the equations of motion, the sensitivity formulations to the DOFs in the subcomponent D_{p} pertain to *complete* DOF-vectors $\underline{\phi}^D$ and $\underline{\rho}^D$ in the blade component D, with also translations in all three directions. That's why the expressions below include 3×3 zero-matrices $\mathbf{O}_m$ for the DOFs on the m^{th} blade element $(m = 1, 4, 5, 6)$:

$$\begin{aligned}
\frac{\partial \underline{v}^{D_3^{\mathrm{a}}}}{\partial \underline{\dot{\phi}}^D} &= [\mathbf{O}_1 \quad \mathrm{J}_{i=2}^{3}(\sum_{m=i}^{3} {}^{D_k}\bar{\Phi}^{D_m} \cdot \mathrm{J}_{v=1}^{3}(\\
&\quad {}^{D_m}\bar{\Phi}^{D_i} \cdot {}^{D_i}\underline{\bar{\Phi}}_v^{D_i^{\iota \mathrm{r}}} \times {}^{D_m^{\ominus}}\underline{r}^{D_{m|3}^{\oplus|\mathrm{a}}})) \quad \mathbf{O}_4 \ldots \mathbf{O}_N] \\
\frac{\partial \underline{v}^{D_3^{\mathrm{a}}}}{\partial \underline{\dot{\varrho}}^D} &= \left[\mathbf{O}_1 \quad \mathrm{J}_{i=2}^{3}({}^{D_3}\bar{\Phi}^{D_i} \cdot {}^{D_i}\bar{\Phi}^{D_i^{\iota \mathrm{t}}}) \quad \mathbf{O}_4 \ldots \mathbf{O}_N\right]
\end{aligned} \tag{21}$$

The sensitivity $\partial \underline{v}^{D_3^{\mathrm{a}}}/\partial \underline{\phi}^D$ accounts for the orientation variation of the local coordinate system on D_3 relative to the flange.

$$\begin{aligned}
\frac{\partial \underline{v}^{D_3^{\mathrm{a}}}}{\partial \underline{\phi}^D} &= \Big[\mathbf{O}_1 \quad \mathrm{J}_{i=2}^{k}\Big(\mathrm{J}_{v=1}^{3}\Big(\frac{\partial {}^{D_3}\Phi^{D_1}}{\partial \phi_v^{D_i}}\underline{\bar{v}}^{D_1^{\oplus}} + \frac{\partial {}^{D_3}\Phi^{D_1}}{\partial \phi_v^{D_i}}\underline{\bar{\omega}}^{D_1} \times \\
&\quad {}^{D_0^{\oplus}}\underline{\bar{r}}^{D_3^{\mathrm{a}}} + \underline{\bar{\omega}}^{D_3} \times \sum_{m=2}^{i-1} \frac{\partial {}^{D_3}\Phi^{D_m}}{\partial \phi_v^{D_1}} \cdot {}^{D_m^{\ominus}}\underline{\bar{r}}^{D_m^{\oplus}}\Big)\Big) \quad \mathbf{O}_4 \ldots \mathbf{O}_N\Big]
\end{aligned} \tag{22}$$

The matrices ${}^{D_i}\bar{\Phi}^{D_i^{\iota \mathrm{r}}}$ and ${}^{D_i}\bar{\Phi}^{D_i^{\iota \mathrm{t}}}$ map the time derivatives of the angular and linear DOFs to the angular velocity and linear velocity increase of D_i relative to D_{i-1}, expressed in coordinates along local unit vectors $\vec{e}_{(x,y,z)}^{\,D_i}$. These matrices are established from columns of products of three, two or one incremental transformation matrices like Φ_{z} for the first, second and third bottom-up ranked rotation and corresonding translation respectively. See §A.3.3 for further explanation.

The sensitivity $\partial {}^{D_3}\Phi^{D_1}/\partial \phi_v^{D_i}$ of the transformation matrix over the elements D_2 and D_3 to the angular DOFs is clarified via the flatwise rotation variation in element D_2. As mentioned above, this concerns the second bottom-up ranked rotation in D_2:

$$\begin{aligned}
\frac{\partial^{D_3}\Phi^{D_1}}{\partial \phi_2^{D_2}} &= {}^{D_3}\bar{\Phi}^{D_2} \cdot \Phi_{\mathrm{x}}(\bar{\phi}_3^{D_2}) \cdot \frac{\mathrm{d}\Phi_{\mathrm{z}}}{\mathrm{d}\phi}(\bar{\phi}_2^{D_m}) \cdot \Phi_{\mathrm{y}}(\bar{\phi}_1^{D_2}) \,, \\
&\text{with: } \frac{\mathrm{d}\Phi_{\mathrm{z}}}{\mathrm{d}\phi}(\bar{\phi}) = \begin{pmatrix} -\sin\bar{\phi} & \cos\bar{\phi} & 0 \\ -\cos\bar{\phi} & -\sin\bar{\phi} & 0 \\ 0 & 0 & 0 \end{pmatrix}
\end{aligned} \tag{23}$$

Similar expressions hold for the sensitivity to the other angular DOFs.

The average place vector from the root exit (=flange entry) to the aerodynamic conversion point on D_3 is obtained by:

$${}^{D_0^{\oplus}}\underline{\bar{r}}^{D_3^{\mathrm{a}}} = {}^{D_3}\bar{\Phi}^{D_1} \,.\, {}^{D_1^{\ominus}}\underline{r}^{D_1^{\oplus}} + {}^{D_3}\bar{\Phi}^{D_2} \,.\, {}^{D_2^{\ominus}}\underline{r}^{D_2^{\oplus}} + {}^{D_3^{\ominus}}\underline{r}^{D_3^{\mathrm{a}}} \tag{24}$$

The derivation principles for the expressions of the kinematic variables are stepwise introduced in §A.2.1 and §A.3.3 respectively.

Equations of motion

Now, let we consider equation (14) and (15) in coordinates along the local coordinate system on D_3. The normal differential vector equations can be written in general form by combining the aerodynamic and gravity loads to external loads:

$$\begin{aligned}
{}^{D_3^{\ominus}}\underline{\dot{h}}^{D_3} &= {}^{\mathrm{RS}}\underline{t}^{D_3^{\ominus}} + {}^{\mathrm{EX}}\underline{t}^{D_3^{\ominus}} + {}^{D_4^{\ominus}}\underline{t}^{D_3^{\oplus}} + {}^{D_3^{\ominus}}\underline{r}^{D_3^{\oplus}} \times {}^{D_4^{\ominus}}\underline{f}^{D_3^{\oplus}} \\
\underline{\dot{p}}^{D_3} &= {}^{\mathrm{RS}}\underline{f}^{D_3^{\ominus}} + {}^{\mathrm{EX}}\underline{f}^{D_3^{\ominus}} + {}^{D_4^{\ominus}}\underline{f}^{D_3^{\oplus}}
\end{aligned} \tag{25}$$

For the assessment of the equilibrium and the derivation of a linear dynamic model description these equations are to subdivided into mean values and *linear* dependencies on varations of kinematic and input variables.

The rate of change in the (biased) angular impulse and the linear impulse is written as a function of mean and variations of the angular velocity and acceleration, and the linear acceleration (expression for these kinematic variables are similar to those for the linear velocity of point D_3^{a} by equation (16)):

$$\begin{aligned}
{}^{D_3^{\ominus}}\underline{\dot{h}}^{D_3} &= {}^{D_3^{\ominus}}\underline{r}^{D_3^*} \times m^{D_3}(\underline{\bar{a}}^{D_3^*} + \delta\underline{a}^{D_3^*}) + \boldsymbol{I}^{D_3} \cdot \delta\underline{\alpha}^{D_3} + \\
&\quad \underline{\bar{\omega}}^{D_3} \times \boldsymbol{I}^{D_3} \cdot \underline{\bar{\omega}}^{D_3} + \underline{\bar{\omega}}^{D_3} \times \boldsymbol{I}^{D_3} \cdot \delta\underline{\omega}^{D_3} + \delta\underline{\omega}^{D_3} \times \boldsymbol{I}^{D_3} \cdot \underline{\bar{\omega}}^{D_3} \\
\underline{\dot{p}}^{D_3} &= m^{D_3} \cdot (\underline{\bar{a}}^{D_3^*} + \delta\underline{a}^{D_3^*})
\end{aligned} \tag{26}$$

The inertia matrix $\boldsymbol{I}^{D_3}$ contains the inertia moments and products relative to the centre of gravity of D_3 and applies along the axes of the final coordinate system of D_3. The matrix $\boldsymbol{I}^{D_3}$ follows from the principle moments of inertia $J_{x,y,z}^{D_3}$ for the concerning blade element.

The aerodynamic force and torque loads ${}^{\mathrm{a}}\underline{f}^{D_3^{\mathrm{a}}}$ and ${}^{\mathrm{a}}\underline{t}^{D_3^{\mathrm{a}}}$ are derived from the distributed force and

torque loading over the elements by:

$$
\begin{aligned}
{}^{\mathrm{a}}\underline{f}^{D_3^{\mathrm{a}}} &= \sum_{j=-1}^{1} {}^{D_3}\Phi^{D_{3+j}^{\mathrm{cv}}} \cdot {}^{\mathrm{a}}G^{\mathrm{F}}_{\mathrm{fq}_{3,j}} \cdot {}^{\mathrm{a}}\underline{q}_{\mathrm{f}}^{D_{3+j}^{\mathrm{cv}}} \\
{}^{\mathrm{a}}\underline{t}^{D_3^{\mathrm{a}}} &= {}^{D_3}\Phi^{D_3^{\mathrm{cv}}}\,{}^{\mathrm{a}}G^{\mathrm{M}}_{\mathrm{tq}_3}\,{}^{\mathrm{a}}\underline{q}_{\mathrm{t}}^{D_3^{\mathrm{cv}}} + \sum_{j=-1}^{1} {}^{D_3}\Phi^{D_{3+j}^{\mathrm{cv}}}\,{}^{\mathrm{a}}G^{\mathrm{F}}_{\mathrm{tq}_{3,j}}\,{}^{\mathrm{a}}\underline{q}_{\mathrm{f}}^{D_{3+j}^{\mathrm{cv}}}
\end{aligned}
\tag{27}
$$

The matrices ${}^{\mathrm{a}}G^{\mathrm{F}}_{\mathrm{fq}_{3,j}}$, ${}^{\mathrm{a}}G^{\mathrm{F}}_{\mathrm{tq}_{3,j}}$ and ${}^{\mathrm{a}}G^{\mathrm{M}}_{\mathrm{tq}_3}$ are chosen such that the 'beam bending equivalence' as discussed near equation (13) is maintained (see App. C in [20]). The matrices ${}^{D_3}\Phi^{D_{3+j}^{\mathrm{cv}}}$ $(j = -1, 0, 1)$ map the normal and tangentially directed distributed force loads to flat- and edgwise oriented components.

The aerodynamic loading is based on basic application of lift-, drag- and moment polaires, as e.g. described in [11]. Vector expressions apply for the distributed force and torque loads. The normal and tangential force components are in the first and third location of coordinate vector ${}^{\mathrm{a}}\underline{q}_{\mathrm{f}}^{D_3^{\mathrm{cv}}}$, while *minus* the nose-up positive aerodynamic pitch torque is in the second location of ${}^{\mathrm{a}}\underline{q}_{\mathrm{t}}^{D_3^{\mathrm{cv}}}$.

Note that the variations in the concentrated aerodynamic loads are determined by the variations $\delta\,{}^{\mathrm{a}}\underline{q}_{\mathrm{f}}^{D_3^{\mathrm{cv}}}$ and $\delta\,{}^{\mathrm{a}}\underline{q}_{\mathrm{t}}^{D_3^{\mathrm{cv}}}$ as well as by products of matrix variation $\delta\,{}^{D_3}\Phi^{D_{3+j}^{\mathrm{cv}}}$ and mean distributed loads ${}^{\mathrm{a}}\overline{\underline{q}}_{\mathrm{f}}^{D_3^{\mathrm{cv}}}$ and ${}^{\mathrm{a}}\overline{\underline{q}}_{\mathrm{f}}^{D_3^{\mathrm{cv}}}$.

With the 'aerodynamic coefficient matrix' $\boldsymbol{C}_{\mathrm{LD}}$ and 'aerodynamic coefficient vector' $\underline{\boldsymbol{C}}_{\mathrm{M}}$ defined by:

$$
\boldsymbol{C}_{\mathrm{LD}}^{D_3} = \begin{pmatrix} C_{\mathrm{D}} & 0 & -C_{\mathrm{L}} \\ 0 & 0 & 0 \\ C_{\mathrm{L}} & 0 & C_{\mathrm{D}} \end{pmatrix}^{D_3}; \quad \underline{\boldsymbol{C}}_{\mathrm{M}}^{D_3} = \begin{bmatrix} 0 \\ -C_{\mathrm{M}} \\ 0 \end{bmatrix}^{D_3}
\tag{28}
$$

the following linearised expressions hold for ${}^{\mathrm{a}}\underline{q}_{\mathrm{f}}^{D_3^{\mathrm{cv}}}$ and ${}^{\mathrm{a}}\underline{q}_{\mathrm{t}}^{D_3^{\mathrm{cv}}}$ (first term in RHS represent mean values):

$$
\begin{aligned}
{}^{\mathrm{a}}\underline{q}_{\mathrm{f}}^{D_3^{\mathrm{cv}}} &= \tfrac{1}{2}\rho c^{D_3} \cdot ||\underline{\bar{u}}^{D_3}|| \cdot \boldsymbol{C}_{\mathrm{LD}}^{D_3}(\bar{\phi}_{\mathrm{a}"}^{D_3}) \cdot \underline{\bar{u}}^{D_3} + \\
&\quad \tfrac{1}{2}\rho c^{D_3} \cdot \left(\bar{\boldsymbol{C}}_{\mathrm{LD}}^{D_3} \cdot \frac{\underline{\bar{u}}^{D_3} \cdot \underline{\bar{u}}^{D_3\,\mathrm{T}}}{||\underline{\bar{u}}^{D_3}||} + ||\underline{\bar{u}}^{D_3}|| \cdot \bar{\boldsymbol{C}}_{\mathrm{LD}}^{D_3} \right) \cdot \delta\underline{u}^{D_3} + \\
&\quad \tfrac{1}{2}\rho c^{D_3} \cdot ||\underline{\bar{u}}^{D_3}|| \cdot \left. \frac{\mathrm{d}\boldsymbol{C}_{\mathrm{LD}}^{D_3}}{\mathrm{d}\phi_{\mathrm{a}"}^{D_3}} \right|_{\bar{\phi}_{\mathrm{a}"}^{D_3}} \cdot \underline{\bar{u}}^{D_3} \cdot \delta\phi_{\mathrm{a}"}^{D_3}
\end{aligned}
\tag{29}
$$

$$
\begin{aligned}
{}^{\mathrm{a}}\underline{q}_{\mathrm{t}}^{D_3^{\mathrm{cv}}} &= \tfrac{1}{2}\rho (c^{D_3})^2 \cdot ||\underline{\bar{u}}^{D_3}||^2 \cdot \underline{\boldsymbol{C}}_{\mathrm{M}}^{D_3}(\bar{\phi}_{\mathrm{a}"}^{D_3}) + \\
&\quad \tfrac{1}{2}\rho (c^{D_3})^2 \cdot \left(2\underline{\bar{\boldsymbol{C}}}_{\mathrm{M}}^{D_3} \cdot \underline{\bar{u}}^{D_3\,\mathrm{T}} \right) \cdot \delta\underline{u}^{D_3} + \\
&\quad \tfrac{1}{2}\rho ({}_c D_3)^2 \cdot ||\underline{u}^{D_3}||^2 \cdot \left. \frac{\mathrm{d}\underline{\boldsymbol{C}}_{\mathrm{M}}^{D_3}}{\mathrm{d}\phi_{\mathrm{a}"}^{D_3}} \right|_{\bar{\phi}_{\mathrm{a}"}^{D_3}} \cdot \delta\phi_{\mathrm{a}"}^{D_3}
\end{aligned}
\tag{30}
$$

with chord length c^{D_3} and the mass density of air ρ.

The vector $\underline{u}^{D_3}$ contains the normal relative wind speed $U_{\mathrm{n}}^{D_3}$ on D_3 in the first location and *minus* the leadwise relative wind speed $-U_{\ell}^{D_3}$ in the third location. It is the sum of the following velocities in D_3^{a}:

- normal wind speed,
- modulation of mean oblique wind speed,
- undisturbed tangential wind speed variation,
- minus axial and plus tangential induction speeds,
- minus structural velocity $\underline{v}^{D_3^{\mathrm{a}}}$.

The angle of attack $\phi_{\mathrm{a}"}$ stands for the geometric angle of attack on 1/4-chord, corrected with the term $\frac{1}{2}\,c^{D_3}/r^{D_3} \cdot \sin\beta^{D_3}$ for the cone angle. The used linearised expression is:

$$
\begin{aligned}
\phi_{\mathrm{a}"}^{D_3} &= \arctan\frac{\bar{U}_{\mathrm{n}}^{D_3}}{\bar{U}_{\ell}^{D_3}} - \bar{\phi}_{\mathrm{set}}^{D_3} + \frac{1/2\,c^{D_3}}{r^{D_3}} \cdot \sin\beta^{D_3} + \\
&\quad \frac{(\underline{\bar{u}}^{D_3})^{\mathrm{T}}}{||\underline{\bar{u}}^{D_3}||^2} \cdot \begin{pmatrix} 0 & 0 & 1 \\ 0 & 0 & 0 \\ -1 & 0 & 0 \end{pmatrix} \delta\underline{u}^{D_3} + \\
&\quad \sum_{i=1}^{3}\sum_{v=1}^{3} \left(-\frac{\partial\phi_{\mathrm{set}}^{D_3}}{\partial\phi_v^{D_i}} + \frac{1/2\,c^{D_3}}{r^{D_3}} \cdot \cos\bar{\beta}^{D_3} \cdot \frac{\partial\beta^{D_3}}{\partial\phi_v^{D_i}} \right) \cdot \delta\phi_v^{D_i}
\end{aligned}
\tag{31}
$$

The (blade element specific) cone angle β^{D_3} and setting angle $\phi_{\mathrm{set}}^{D_3}$ vary dynamically. Their variation is considered relative to the rotor centre. So, angular motion of the rotor centre caused by shaft or tower deformation does *not* affect the setting and cone angle!

The setting angle is mainly determined by the aerodynamic pitch angle of the rotor blade and the (controlled) pitch angle at the blade flange entry. However, prebend and average deformation may link leadwise deformation variations to setting angle variations. This dependency is part of the sensitivity function of the setting angle to the angular DOFs in the rotor blade.

The visco-elastic bending and torsion torques in $D_3^{\ominus}$ are simply proportional to the angular DOFs. Since all DOFs are modelled in the entry point of the blade elements, the translation of the shear centre relative to the foregoing element depends on the linear *as well as on angular* bending DOFs. A heuristic approximation tells that for the total relative translation $\delta\underline{\hat{\rho}}^{D_3}$ holds:

$$
\delta\begin{bmatrix} \hat{\rho}_x^{D3} \\ \hat{\rho}_y^{D3} \\ \hat{\rho}_z^{D3} \end{bmatrix} = \delta\begin{bmatrix} \rho_x^{D3} \\ \rho_y^{D3} \\ \rho_z^{D3} \end{bmatrix} + \delta\begin{bmatrix} \phi_x^{D3} \\ \phi_y^{D3} \\ \phi_z^{D3} \end{bmatrix} \times {}^{D_3^{\ominus}}\underline{r}^{D_3^{\mathrm{s}}}
\tag{32}
$$

The elastic linear bending loads are obtained from

a slightly modified expression for $\delta\hat{\underline{\rho}}^{D_3}$ in order to take into account the average rotation increments.

The heuristic expressions for the elastic responsive loads in $D_3^{\ominus}$ are:

$$
\begin{aligned}
{}^{\mathrm{RS}}\underline{t}^{D_3^{\ominus}} &= -\begin{pmatrix} s_{\mathrm{r_x}}^{D_3} & 0 & 0 \\ 0 & s_{\mathrm{r_y}}^{D_3} & 0 \\ 0 & 0 & s_{\mathrm{r_z}}^{D_3} \end{pmatrix} \cdot \begin{bmatrix} \hat{\phi}_x^{D3} \\ \hat{\phi}_y^{D3} \\ \hat{\phi}_z^{D3} \end{bmatrix} + {}^{D_3^{\ominus}}\underline{r}^{D_3^{\mathrm{s}}} \times {}^{\mathrm{RS}}\underline{f}^{D_3^{\ominus}} \\
{}^{\mathrm{RS}}\underline{f}^{D_3^{\ominus}} &= -\begin{pmatrix} s_{\mathrm{t_x}}^{D_3} & 0 & 0 \\ 0 & s_{\mathrm{t_y}}^{D_3} & 0 \\ 0 & 0 & s_{\mathrm{t_z}}^{D_3} \end{pmatrix} \cdot \begin{bmatrix} \hat{\rho}_x^{D3} \\ \hat{\rho}_y^{D3} \\ \hat{\rho}_z^{D3} \end{bmatrix}
\end{aligned}
\tag{33}
$$

The viscous reactions are obtained by replacing ϕ_x by $\dot{\phi}_x$ and $s_{\mathrm{r_x}}$ by $d_{\mathrm{r_x}}$ etc. The dampers are also not included in figure 14. Note that the pitch-wise angular DOF in the flange element D_1 can be speficied for a visco-elastic responsive torque or for controllable responsive torque.

Note that angular displacements $\hat{\phi}_{(.)}$ do *not* include the configuration angles from coning, skewness and prebend but *do* include both the average and dynamic deformation.

The gravity forces have a mean coordinate perpendicular to the rotor plane and periodic components in lead and radial direction of the rotor blades. The periodic components on the rotor blades are governed via an explict input variable; if it is active, compensation loads are to be injected in the entry point of the support structure (see §A.3.2). The mean component and variations due to orientation change relative to the mean component are always taken into account unless zero-gravitation is specified. See §A.2.1 and §A.3.3 for explicit expressions for the rotor shaft and the tower.

The expressions for the loads by the next element D_4 in the exit point of D_3 are composed as the difference between the loading on D_4 and the consumed rate of change of impulse by D_4.

The coordinate system independent vector expressions for the feedthrough loads on element D_3 from D_4 are as follows:

$$
\begin{aligned}
{}_{D_4}\vec{t}^{\,D_3^{\oplus}} &= -{}^{D_4^{\ominus}}\dot{\vec{h}}^{D_4} + {}_{D_5}\vec{t}^{\,D_4^{\oplus}} + {}^{D_4^{\ominus\rightarrow}}\vec{r}^{\,D_4^{\oplus}} \times {}_{D_5}\vec{f}^{\,D_4^{\oplus}} + \\
&\quad {}^{\mathrm{a}}\vec{t}^{\,D_4^{\mathrm{a}}} + {}^{D_4^{\ominus\rightarrow}}\vec{r}^{\,D_4^{\mathrm{a}}} \times {}^{\mathrm{a}}\vec{f}^{\,D_4^{\mathrm{a}}} + {}^{D_4^{\ominus\rightarrow}}\vec{r}^{\,D_4^{*}} \times {}^{\mathrm{g}}\vec{f}^{\,D_4^{*}} \\
{}_{D_4}\vec{f}^{\,D_3^{\oplus}} &= -\dot{\vec{p}}^{D_4} + {}_{D_5}\vec{f}^{\,D_4^{\oplus}} + {}^{\mathrm{a}}\vec{f}^{\,D_4^{\mathrm{a}}} + {}^{\mathrm{g}}\vec{f}^{\,D_4^{*}}
\end{aligned}
\tag{34}
$$

The expressions in coordinates for these feedthrough loads are similar to those discussed in the treatment of the equation of motions of D_3.

A.1.2 Pitch servo actuator submodel D_{c}

Figure 15 shows the layout of the submodel for the pitch servo actuator. The interaction with the blade flange submodel is included. A feed-

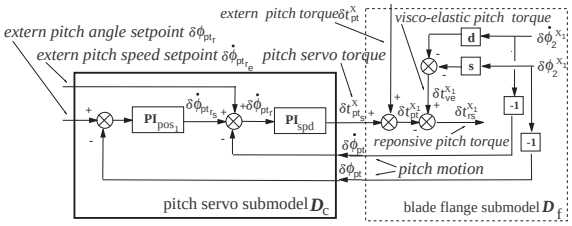

Figure 15: *Pitch servo acutator submodel*

back scheme applies for the pitch position and the pitch speed. The feedback laws in both the outer position loop and the inner speed loop exist of smoothed proportional-integral action (PI). The transfer functions are given by (operator s implies differentiation):

$$
\delta t_{\mathrm{pt_s}} = \frac{K_{\mathrm{v}} \cdot (1 + \frac{1}{\tau_{\mathrm{v}} s})}{(\tau_{\mathrm{v}} s/\gamma_{\mathrm{v}} + 1)} \cdot (\delta\dot{\phi}_{\mathrm{pt_{r_s}}} + \delta\dot{\phi}_{\mathrm{pt_{r_e}}} - \delta\dot{\phi}_{\mathrm{pt}})
\tag{35}
$$

with

$$
\delta\dot{\phi}_{\mathrm{pt_{r_s}}} = \frac{K_{\mathrm{p}} \cdot (1 + \frac{1}{\tau_{\mathrm{p}} s})}{(\tau_{\mathrm{p}} s/\gamma_{\mathrm{p}} + 1)} \cdot (\delta\phi_{\mathrm{pt_r}} - \delta\phi_{\mathrm{pt}})
\tag{36}
$$

TURBU includes a computation scheme for the derivation of the gain and time constants K_{v}, τ_{v}, K_{p}, τ_{p} from specified bandwidths and damping rates for the inner speed loop and outer position loop. The feedback loops can be de-activated by specifying '0 Hz bandwidth values'. So, it also possible to apply pitch *speed* servo control with setpoint $\delta\dot{\phi}_{\mathrm{pt_e}}$ or to apply an external pitch servo actuator that provides the pitching torque $\delta t_{\mathrm{pt_e}}$.

The denumerator terms represent first order low pass filters that accomplish the smoothing property of the PI-feedback laws. The filter frequency of these filters amounts to $\gamma_{\mathrm{v}}/\tau_{\mathrm{v}}$ and $\gamma_{\mathrm{p}}/\tau_{\mathrm{p}}$ rad/s. The smoothing factors γ_{v} and γ_{p} are much larger than 1 (typical $\gamma_{\mathrm{v}} = 3$ and $\gamma_{\mathrm{p}} = 10$; γ_{v} not so large in order to avoid undesired fast eigenmotions).

A.1.3 Unsteady aerodynamics submodel D_{a}

Submodel D_{a} provides dynamic additions to the aerodynamic profile coefficients for all N blade elements. The model equations are obtained by linearisation of the heuristic model for unsteady dependency of the lift coefficient on the angle of

attack ($C_\ell(\alpha)$) according to Snel [12]. This yields the following first order linear differnetaion equation for the unsteady variation $\Delta C_{\ell_{\rm us}}$ for a blade element:

$$\tau \cdot \Delta\dot{C}_{\ell_{\rm us}} + C_{10} \cdot \Delta C_{\ell_{\rm us}} = \tau \cdot \left(2\pi \cos 2\pi(\overline{\alpha} - \alpha_0) - \overline{\frac{\mathrm{d}C_{\ell_{\rm qs}}}{\mathrm{d}\alpha}}\right) \dot{\alpha} \tag{37}$$

The time constant τ and coefficient C_{10} are determined by

$$\begin{aligned} \tau &= c/(2\sqrt{\overline{u}_{\rm n}^2 + \overline{u}_\ell^2}) \\ C_{10} &= (1 + \tfrac{1}{2}|2\pi \sin(\overline{\alpha} - \alpha_0) - C_{\ell_{\rm qs}}(\overline{\alpha})|)/8 \end{aligned} \tag{38}$$

The angle of attack α_0 implies the value for zero-lift.

When we define parameters K and G by:

$$\begin{aligned} K &= C_{10}/\tau \\ G &= 2\pi \cdot \cos 2\pi(\overline{\alpha} - \alpha_0) - \overline{\frac{\mathrm{d}C_{\ell_{\rm qs}}}{\mathrm{d}\alpha}} \end{aligned} \tag{39}$$

the linearised equation can be written as:

$$\Delta\dot{C}_{\ell_{\rm us}} = -K \cdot \Delta C_{\ell_{\rm us}} + G \cdot \dot{\alpha} \tag{40}$$

Define the state variable z by:

$$z = \Delta C_{\ell_{\rm us}} - G \cdot \alpha \tag{41}$$

It is now allowed to transform the governing equation for the unsteady part of the lift coefficient into the following first order state space model:

$$\begin{aligned} \dot{z} &= -K \cdot z - K \cdot G \cdot \alpha \\ \Delta C_{\ell_{\rm us}} &= z + G \cdot \alpha \end{aligned} \tag{42}$$

A.2 Drive-train equations

A.2.1 Rotor shaft & hub submodel $R_{\rm r}$

The rotor shaft & hub is considered to behave deformable as concerns the rotor shaft and undeformable as concerns the hub. Figure 16 shows the physical layout and the vector variables in the model element layout of $R_{\rm r}$. Axi-symmetry is assumed for the shaft.

The elasticity of the shaft is modelled via up to six DOFs with visco-elastic responsive loads in the shaft's entry point $R_{\rm r}^{\ominus}$. We chose to let coincide this entry point with the exit point $R_{\rm r}^{\oplus}$ *in the rotor centre* $R_{\rm r}^{\rm c}$. Together with the inclusion of the main bearing in the bending behaviour, the chosen location of the entry and exit point necessates to include cross couplings between the linear displacement and the angular visco-elastic reaction in a bending direction and vice versa. The

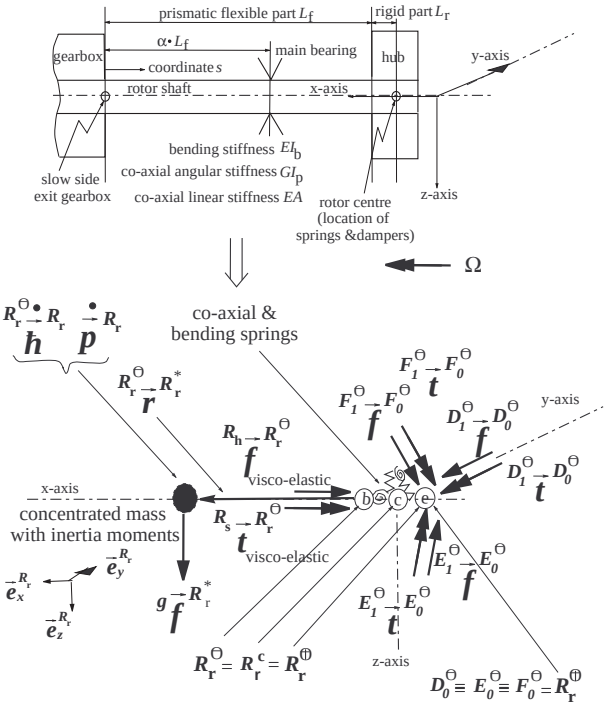

Figure 16: *Equation of motion governing vector variables for rotor shaft & hub submodel*

mass, inertia moments and location of the centre of gravity and the bending, torsion and axial stiffness follow from (weigthed) integration of the shaft cross section data over the shaft-axis.

The coordinate system independent vector expressions for the equations of motion of the rotor shaft & hub element $R_{\rm r}$ are the following:

$$\begin{aligned} {}^{R_{\rm r}^{\ominus}}\dot{\vec{h}}^{R_{\rm r}} &= {}^{\rm RS}\vec{t}^{\,R_{\rm r}^{\ominus}} + {}^{D_1^{\ominus}}\vec{t}^{\,D_0^{\ominus}} + {}^{E_1^{\ominus}}\vec{t}^{\,E_0^{\ominus}} + {}^{F_1^{\ominus}}\vec{t}^{\,F_0^{\ominus}} + {}^{R_{\rm r}^{\rm c}}\vec{r}^{\,R_{\rm r}^*} \times {}^{\rm g}\vec{f}^{\,R_{\rm r}^*} \\ \dot{\vec{p}}^{R_{\rm r}} &= {}^{\rm RS}\vec{f}^{\,D_3^{\ominus}} + {}^{D_1^{\ominus}}\vec{f}^{\,D_0^{\ominus}} + {}^{E_1^{\ominus}}\vec{f}^{\,E_0^{\ominus}} + {}^{F_1^{\ominus}}\vec{f}^{\,F_0^{\ominus}} + {}^{\rm g}\vec{f}^{\,R_{\rm r}^*} \end{aligned} \tag{43}$$

For the angular and linear impulse of the element $R_{\rm r}$ holds (no coordinate system reference):

$$\begin{aligned} {}^{R_{\rm r}^{\rm c}}\dot{\vec{h}}^{R_{\rm r}} &= {}^{R_{\rm r}^{\rm c}}\vec{r}^{\,R_{\rm r}^*} \times \dot{\vec{p}}^{R_{\rm r}} + \boldsymbol{I}^{R_{\rm r}} \bullet \vec{\alpha}^{R_{\rm r}} + \vec{\omega}^{R_{\rm r}} \times \boldsymbol{I}^{R_{\rm r}} \bullet \vec{\omega}^{R_{\rm r}} \\ \dot{\vec{p}}^{R_{\rm r}} &= m^{R_{\rm r}} \vec{a}^{\,R_{\rm r}^*} \end{aligned} \tag{44}$$

First, the evolution of the kinematic variables over the main rotation and the DOFs in the drive-train is considered (see also §A.3.3). Afterwards, we continue with the formulation of the equations of motion as normal differential vector equations along the local coordinate system of $\vec{e}_{(x,y,z)}^{\,R_{\rm r}}$.

Kinematics drive-train

We chose the exit point of the support structure to

coincide with the rotor centre. The linearised expressions for the coordinates along $\vec{e}^{\,R_\mathrm{r}}_{(x,y,z)}$ of the linear velocity and acceleration $\underline{v}^{R^\mathrm{s}_\mathrm{r}}$, $\underline{a}^{R^\mathrm{s}_\mathrm{r}}$ in the rotor centre *before the effectuation of the DOFs* of R_r, so at slow shaft exit of the gearbox, are then obtained by just modulating the corresponding variables that leave the support structure The modulation occurs with the average rotor speed $\bar{\Omega}$:

$$\begin{aligned} \underline{v}^{R^\mathrm{s}_\mathrm{r}} &= \Phi_\mathrm{x}(\bar{\Omega}t)\cdot\underline{v}^{R^\oplus_\mathrm{h}} \\ \underline{a}^{R^\mathrm{s}_\mathrm{r}} &= \Phi_\mathrm{x}(\bar{\Omega}t)\cdot\underline{a}^{R^\oplus_\mathrm{h}} \end{aligned} \tag{45}$$

The angular velocity $\underline{\omega}^{R^\mathrm{s}_\mathrm{r}}$ at the gearbox slow exit is also obtained by modulation of the corresponding variable on the support structure, but it includes in addition the average rotational speed $\bar{\Omega}$ and its variation $\delta\Omega$ as the effect of the generator rotor DOF ($\delta\Omega = \dot{\phi}_x^{R_\mathrm{f}}/i_\mathrm{gb}$):

$$\underline{\omega}^{R^\mathrm{s}_\mathrm{r}} = \Phi_\mathrm{x}(\bar{\Omega}t)\cdot\underline{\omega}^{R_\mathrm{h}} + \begin{bmatrix}\bar{\Omega}\\0\\0\end{bmatrix} + \begin{bmatrix}\delta\Omega\\0\\0\end{bmatrix} \tag{46}$$

The expression for the angular acceleration $\underline{\omega}^{R^\mathrm{s}_\mathrm{r}}$ contains similar terms (2^nd time derivatives, but also a vector product with the average rotational velocity):

$$\underline{\alpha}^{R^\mathrm{s}_\mathrm{r}} = \Phi_\mathrm{x}(\bar{\Omega}t)\cdot\underline{\alpha}^{R_\mathrm{h}} + \begin{bmatrix}\delta\dot{\Omega}\\0\\0\end{bmatrix} + (\Phi_\mathrm{x}(\bar{\Omega}t)\cdot\underline{\omega}^{R_\mathrm{h}}) \times \begin{bmatrix}\bar{\Omega}\\0\\0\end{bmatrix} \tag{47}$$

These expressions follow from the *addition theorem for angular velocities* and the theorem on time-differentiation of vectors fixed in a rigid body, which enables to obtain the first derivative via a vector product ([10], chapter 2). A reformulation of these theorems for the vectors here involved yields (reference frame G in time derivatives ${}^{(G)}\mathrm{d}(.)/\mathrm{d}t$ implies the fixed world):

$$\begin{aligned} \vec{\omega}^{R_\mathrm{s}} &= {}_G\vec{\omega}^{R_\mathrm{h}} + {}_{R_\mathrm{h}}\vec{\omega}^{R_\mathrm{s}} \\ &= \vec{\omega}^{R_\mathrm{h}} + (\bar{\Omega}+\delta\Omega)\ \vec{e}_x^{\,R_\mathrm{h}} \\ \vec{\alpha}^{R_\mathrm{s}} &= {}^{(G)}\frac{\mathrm{d}}{\mathrm{d}t}\left({}_G\vec{\omega}^{R_\mathrm{h}}\right) + {}^{(G)}\frac{\mathrm{d}}{\mathrm{d}t}\left({}_{R_\mathrm{h}}\vec{\omega}^{R_\mathrm{s}}\right) \\ &= {}_G\vec{\alpha}^{R_\mathrm{h}} + {}^{(R_\mathrm{h})}\frac{\mathrm{d}}{\mathrm{d}t}\left({}_{R_\mathrm{h}}\vec{\omega}^{R_\mathrm{s}}\right) + {}_G\vec{\omega}^{R_\mathrm{h}} \times {}_{R_\mathrm{h}}\vec{\omega}^{R_\mathrm{s}} \\ &= \vec{\alpha}^{R_\mathrm{h}} + \delta\dot{\Omega}\ \vec{e}_x^{\,R_\mathrm{h}} + \vec{\omega}^{R_\mathrm{h}} \times (\bar{\Omega}+\delta\Omega)\ \vec{e}_x^{\,R_\mathrm{h}} \end{aligned} \tag{48}$$

Linearisation of the vector product in the last expression yields $\vec{\omega}^{R_\mathrm{h}} \times \bar{\Omega}\ \vec{e}_x^{\,R_\mathrm{h}}$. The unit vector $\vec{e}_x^{\,R_\mathrm{h}}$ remains unchanged in the rotating frame of reference at the gearbox slow exit.

Application of the two theorems to the DOFs added by the rotor shaft yields for the linear approximations of the angular velocity and acceleration (use $\underline{\omega}^{R_{\tilde{\mathrm{h}}}}$ for $\Phi_\mathrm{x}(\bar{\Omega}t)\cdot\underline{\omega}^{R_\mathrm{h}}$ etc., read $\ddot{\varphi}_y^{R_\mathrm{r}}$ for $\ddot{\varphi}_y^\mathrm{r}$):

$$\begin{aligned} \underline{\omega}^{R_\mathrm{r}} &= \begin{bmatrix}\bar{\Omega}\\0\\0\end{bmatrix} + \underline{\omega}^{R_{\tilde{\mathrm{h}}}} + \begin{bmatrix}\delta\Omega\\0\\0\end{bmatrix} + \begin{bmatrix}\dot{\varphi}_x^\mathrm{r}\\ \dot{\varphi}_y^\mathrm{r}\\ \dot{\varphi}_z^\mathrm{r}\end{bmatrix} \\ \underline{\alpha}^{R_\mathrm{r}} &= \underline{\alpha}^{R_{\tilde{\mathrm{h}}}} + \begin{bmatrix}\delta\dot{\Omega}\\0\\0\end{bmatrix} + \underline{\omega}^{R_{\tilde{\mathrm{h}}}} \times \begin{bmatrix}\bar{\Omega}\\0\\0\end{bmatrix} + \begin{bmatrix}\ddot{\varphi}_x^\mathrm{r}\\ \ddot{\varphi}_y^\mathrm{r}\\ \ddot{\varphi}_z^\mathrm{r}\end{bmatrix} + \begin{bmatrix}\bar{\Omega}\\0\\0\end{bmatrix} \times \begin{bmatrix}\dot{\varphi}_x^\mathrm{r}\\ \dot{\varphi}_y^\mathrm{r}\\ \dot{\varphi}_z^\mathrm{r}\end{bmatrix} \end{aligned} \tag{49}$$

The expression for the velocity of the centre of gravity of R_r is derived similarly from the theorems ($\rho = \bar{\rho} + \varrho$; ${}^{R^\ominus_\mathrm{r}}\underline{r}^{R^*_\mathrm{r}} = [r_x^*\ \ 0\ \ 0]'$ and $\bar{\rho}_y^\mathrm{r} = 0$, $\bar{\rho}_z^\mathrm{r} = 0$ because of assumed axi-symmetry):

$$\begin{aligned} \underline{v}^{R^*_\mathrm{r}} = \begin{bmatrix}\bar{\Omega}\\0\\0\end{bmatrix} \times \begin{bmatrix}r_x^* + \bar{\rho}_x^\mathrm{r}\\0\\0\end{bmatrix} + \underline{v}^{R^\oplus_{\tilde{\mathrm{h}}}} + \begin{bmatrix}\dot{\varrho}_x^\mathrm{r}\\ \dot{\varrho}_y^\mathrm{r}\\ \dot{\varrho}_z^\mathrm{r}\end{bmatrix} + \\ \begin{bmatrix}\delta\Omega + \dot{\varphi}_x^\mathrm{r}\\ \dot{\varphi}_y^\mathrm{r}\\ \dot{\varphi}_z^\mathrm{r}\end{bmatrix} \times \begin{bmatrix}r_x^*\\0\\0\end{bmatrix} + \begin{bmatrix}\bar{\Omega}\\0\\0\end{bmatrix} \times \begin{bmatrix}\varrho_x^\mathrm{r}\\ \varrho_y^\mathrm{r}\\ \varrho_z^\mathrm{r}\end{bmatrix} \end{aligned} \tag{50}$$

The effect of the linear *position* values $\rho_{(.)}$ on the kinematic variables is **not** carried through in TURBU. However, the effect of the linear *speed* and *acceleration* values $\dot{\varrho}_{(.)}$ and $\ddot{\varrho}_{(.)}$ **is** carried through. Equilibrium assessment pointed out that the linear position values are very much smaller than products of angular position values and typical place vectors.

When terms involving $\underline{\rho}_{(.)}$ are neglected, the expression for the acceleration of the centre of gravity of R_r becomes:

$$\begin{aligned} \underline{a}^{R^*_\mathrm{r}} = \begin{bmatrix}\bar{\Omega}\\0\\0\end{bmatrix} \times \left(\begin{bmatrix}\bar{\Omega}\\0\\0\end{bmatrix} \times \begin{bmatrix}r_x^*\\0\\0\end{bmatrix}\right) + \underline{a}^{R^\oplus_{\tilde{\mathrm{h}}}} + \underline{\alpha}^{R^\oplus_{\tilde{\mathrm{h}}}} \times \begin{bmatrix}r_x^*\\0\\0\end{bmatrix} + \\ 2\underline{\omega}^{R^\oplus_{\tilde{\mathrm{h}}}} \times \left(\begin{bmatrix}\bar{\Omega}\\0\\0\end{bmatrix} \times \begin{bmatrix}r_x^*\\0\\0\end{bmatrix}\right) + \begin{bmatrix}\ddot{\varrho}_x^\mathrm{r}\\ \ddot{\varrho}_y^\mathrm{r}\\ \ddot{\varrho}_z^\mathrm{r}\end{bmatrix} + \begin{bmatrix}\delta\dot{\Omega} + \ddot{\varphi}_x^\mathrm{r}\\ \ddot{\varphi}_y^\mathrm{r}\\ \ddot{\varphi}_z^\mathrm{r}\end{bmatrix} \times \begin{bmatrix}r_x^*\\0\\0\end{bmatrix} + \\ 2\begin{bmatrix}\bar{\Omega}\\0\\0\end{bmatrix} \times \left(\begin{bmatrix}\dot{\varphi}_x^\mathrm{r}\\ \dot{\varphi}_y^\mathrm{r}\\ \dot{\varphi}_z^\mathrm{r}\end{bmatrix} \times \begin{bmatrix}r_x^*\\0\\0\end{bmatrix}\right) \end{aligned} \tag{51}$$

The expressions above are derived by considering the coordinates along $\vec{e}^{\,R_\mathrm{r}}_{(x,y,z)}$ of the coordinate system independent velocity and acceleration:

$$\begin{aligned} \vec{v}^{R^*_\mathrm{r}} &= \vec{v}^{R^\oplus_\mathrm{h}} + {}^{(R_\mathrm{r})}\frac{\mathrm{d}}{\mathrm{d}t}\left({}_{R^\ominus_\mathrm{r}}\vec{r}^{R^*_\mathrm{r}}\right) + \vec{\omega}^{R_\mathrm{r}} \times {}_{R^\ominus_\mathrm{r}}\vec{r}^{R^*_\mathrm{r}} \\ \vec{a}^{R^*_\mathrm{r}} &= \vec{a}^{R^\oplus_\mathrm{h}} + {}^{(R_\mathrm{r})}\frac{\mathrm{d}^2}{\mathrm{d}t^2}\left({}_{R^\ominus_\mathrm{r}}\vec{r}^{R^*_\mathrm{r}}\right) + \vec{\alpha}^{R_\mathrm{r}} \times {}_{R^\ominus_\mathrm{r}}\vec{r}^{R^*_\mathrm{r}} \\ &\quad 2\vec{\omega}^{R_\mathrm{r}} \times {}^{(R_\mathrm{r})}\frac{\mathrm{d}}{\mathrm{d}t}\left({}_{R^\ominus_\mathrm{r}}\vec{r}^{R^*_\mathrm{r}}\right) + \vec{\omega}^{R_\mathrm{r}} \times (\vec{\omega}^{R_\mathrm{r}} \times {}_{R^\ominus_\mathrm{r}}\vec{r}^{R^*_\mathrm{r}}) \end{aligned} \tag{52}$$

It is clear that because of the axi-symmetry a number of terms in the expressions for the velocity and acceleration will be zero. However, the complete expressions are listed since they are fun-

damentally the same for the kinematic variables on the rotor blades.

Equations of motion

Now we return to the equations of motion. The expressions for the angular and linear impulse become:

$$\begin{aligned} {}^{R_r^{\ominus}}\dot{\underline{h}}^{R_r} &= {}^{R_r^{\ominus}}\underline{r}^{R_r^*} \times m^{R_r}\delta\underline{a}^{R_r^*} + \boldsymbol{I}^{R_r}\cdot\delta\underline{\alpha}^{R_r} + \\ &\bar{\underline{\omega}}^{R_r}\times\boldsymbol{I}^{R_r}\cdot\delta\underline{\omega}^{R_r} + \delta\underline{\omega}^{R_r}\times\boldsymbol{I}^{R_r}\cdot\bar{\underline{\omega}}^{R_r} \\ \dot{\underline{p}}^{R_r} &= m^{R_r}\cdot(\bar{\underline{a}}^{R_r^*} + \delta\underline{a}^{R_r^*}) \end{aligned} \tag{53}$$

The terms ${}^{R_r^{\ominus}}\underline{r}^{R_r^*} \times m^{R_r}\bar{\underline{a}}^{R_r^*}$, $\bar{\underline{\omega}}^{R_r}\times\boldsymbol{I}^{R_r}\cdot\bar{\underline{\omega}}^{R_r}$ and $m^{R_r}\cdot\bar{\underline{a}}^{R_r^*}$ do not appear because we now carried through the implications of the axi-symmetry of the rotor shaft & hub.

The force and torque loads from the rotor blades enter the drive train as coordinates along the blade roots' coordinate systems, which are rotated over the azimut offset $\Delta\psi$ along the rotor shaft relative to the coordinate system (0, $\frac{2}{3}\pi$ and $\frac{4}{3}\pi$ for blades D, E and F). If we regroup the loads in the equations of motion as responsive and external loads, the eoms are then formulated as:

$$\begin{aligned} {}^{R_r^{\ominus}}\dot{\underline{h}}^{R_r} &= {}^{\text{RS}}\underline{t}^{R_r^{\ominus}} + {}^{\text{EX}}\underline{t}^{R_r^{\ominus}} \\ \dot{\underline{p}}^{R_r} &= {}^{\text{RS}}\underline{f}^{R_r^{\ominus}} + {}^{\text{EX}}\underline{f}^{R_r^{\ominus}} \end{aligned} \tag{54}$$

with

$$\begin{aligned} {}^{\text{EX}}\underline{t}^{R_r^{\ominus}} &= \sum_{X=D,E,F}\Phi_{\text{x}}(-\Delta\psi_X)\cdot{}^{X_1^{\ominus}}\underline{t}^{X_0^{\ominus}} + \begin{bmatrix} r_x^* \\ 0 \\ 0 \end{bmatrix}\times{}^{\text{g}}\underline{f}^{R_r^*} \\ {}^{\text{EX}}\underline{f}^{R_r^{\ominus}} &= \sum_{X=D,E,F}\Phi_{\text{x}}(-\Delta\psi_X)\cdot{}^{X_1^{\ominus}}\underline{f}^{X_0^{\ominus}} + {}^{\text{g}}\underline{f}^{R_r^*} \end{aligned} \tag{55}$$

The gravity loading coordinates along $\vec{e}^{\,R_r}_{(1,2,3)}$ contain mean, periodic and reactive terms. The approximate expression is

$$\begin{aligned} {}^{\text{g}}\underline{f}^{R_r^*} \quad = \quad & m^{R_r}g\begin{bmatrix}\sin\theta_{\text{tl}}\\0\\0\end{bmatrix} + m^{R_r}g\cos\theta_{\text{tl}}\begin{bmatrix}0\\\sin\bar{\Omega}t\\\cos\bar{\Omega}t\end{bmatrix} + \\ & m^{R_r}g\sin\theta_{\text{tl}}\begin{bmatrix}0&0&0\\0&0&-1\\0&1&0\end{bmatrix}\begin{bmatrix}\phi_x^{R_r}\\\phi_y^{R_r}\\\phi_z^{R_r}\end{bmatrix} + m^{R_r}\Phi_{\text{x}}(\bar{\Omega}t)\cdot\delta\underline{g}_{\text{ori}}^{R_h} \end{aligned} \tag{56}$$

See [20], App. B for the implemented expression in TURBU, in which the operations with the tilt angle θ_{tl} are replaced by transformation matrix from the geographic cooridinate system to the nacelle. The contribution by $\underline{g}_{\text{ori}}^{R_h}$ is caused by orientation variations from dynamic tower bending, which influence the position of the y- and z-axis of the coordinate system on the rotor shaft. See also §A.3.3.

This expression for the gravity loading is fundamentally the same for the rotor blades.

The expressions for the elastic responsive loads in $R_r^{\ominus}$ are (read $s_{\text{tr}_x}^{R_r}$ for s_{tr_x} and $\phi_x^{R_r}$ for ϕ_x etc.):

$$\begin{aligned} {}^{\text{RS}}\underline{t}^{R_r^{\ominus}} &= -\begin{pmatrix} s_{\text{tr}_x} & 0 & 0 \\ 0 & s_{\text{tr}_y} & 0 \\ 0 & 0 & s_{\text{tr}_z}\end{pmatrix}\begin{bmatrix}\phi_x\\\phi_y\\\phi_z\end{bmatrix} - \begin{pmatrix} 0 & 0 & 0 \\ 0 & 0 & s_{\text{tt}_{yz}} \\ 0 & s_{\text{tt}_{zy}} & 0\end{pmatrix}\begin{bmatrix}\rho_x\\\rho_y\\\rho_z\end{bmatrix} \\ {}^{\text{RS}}\underline{f}^{R_r^{\ominus}} &= -\begin{pmatrix} s_{\text{ft}_x} & 0 & 0 \\ 0 & s_{\text{ft}_y} & 0 \\ 0 & 0 & s_{\text{ft}_z}\end{pmatrix}\begin{bmatrix}\rho_x\\\rho_y\\\rho_z\end{bmatrix} - \begin{pmatrix} 0 & 0 & 0 \\ 0 & 0 & s_{\text{fr}_{yz}} \\ 0 & s_{\text{fr}_{zy}} & 0\end{pmatrix}\begin{bmatrix}\phi_x\\\phi_y\\\phi_z\end{bmatrix} \end{aligned} \tag{57}$$

The bending stiffness values ($y-$ and $z-$orientation) are determined under the following constraints, visualised in figure 16 (see [20], Chapter 3):

- reponsive force & torques in rotor centre;
- zero linear displacement in main bearing centre;
- zero angular and linear displacement at slow gearbox exit.

A.2.2 Generator rotor submodel R_{f}

The generator rotor is considered to behave undeformable while a co-axial visco-elastic or controllable angular DOF is allowed. Only the co-axial angular behaviour is taken into account in the submodel. The equation of motion is based on the real fast shaft angular speed.

The co-axial rotational speed of the generator rotor is the sum of the corresponding rotational speed of the nacelle, the variation $\dot{\varphi}_x^{R_f}$ of the rotor itself (the DOF), and the average rotational speed transformed via the gearbox, that is to say $i_{\text{gb}}\bar{\Omega}$.

The generator speed variation is transmitted to the slow shaft of the gearbox, that is to say $\delta\Omega = \dot{\varphi}_x^{R_f}/i_{\text{gb}}$.

A.3 Support structure equations

A.3.1 Gearbox house submodel R_{h}

The gearbox house is considered to behave undeformable while a co-axial visco-elastic or controllable angular DOF is allowed. Only the co-axial angular behaviour is taken into account in the submodel. The full relative rotation $\phi_x^{R_h}$ applies in the equation of motion for R_{h} whereas the rotational speed of the slow gearbox shaft is augmented with the fraction $((i_{\text{gb}}-1)/i_{\text{gb}})$ of $\dot{\varphi}_x^{R_h}$.

A.3.2 Nacelle submodel S_n

The nacelle is considered to behave undeformable while visco-elastic DOFs in all six directions are allowed in the connection point with the tower top (=yaw bearing centre) . The yaw DOF can also be specified 'controllable'. In that case the external yaw torque replaces the visco-elastic responsive behaviour in the yaw DOF.

Except the co-axial moment of inertia, all inertia properties of the the gearbox house R_h and generator rotor R_f are added to those of the nacelle. For the generator rotor this also involves gyrocopic effects because of the average rotation that amounts to $i_\mathrm{gb}\bar{\Omega}$.

A.3.3 Foundation and tower submodels S_f, S_t

The submodels for the foundation and the tower are established from equations of motion that are obtained in the same way as those for the structural submodels X_f and X_p of the rotor blades. The model equations are basicly the same, but are less complicated because we assume that *in the tower axis*:

- the shear and elastic axis coincide;
- the concentrated hydrodynamic loads affect.

In addition there is no average motion of the support structure, so the equations of motion for an element S_k do not include terms derived from $\underline{\omega}\times\boldsymbol{I}\cdot\underline{\omega}$, as *is* the case in equation (26). This vector product now only contains products rotation variations. These 2^nd order terms are neglected in the linear approach.

The masses of the underwater elements may be augmented with the enclosed water mass.

First, the evolution of the kinematic variables over the DOFs in the support structure is considered. Afterwards, equations of motion are formulated as normal differential vector equations along the local coordinate systems of $\vec{e}^{\,S_k}_{(x,y,z)}$.

Kinematics support structure

The angular velocity and acceleration of tower element S_3 have zero mean values and are obtained by:

$$\begin{aligned}\delta\underline{\omega}^{S_3} &= {}^{S_3}\bar{\Phi}^{S_1}\cdot\underline{\omega}^{S_1} + \sum_{i=2}^{3} {}^{S_3}\bar{\Phi}^{S_i}\,.\,{}^{S_i}\bar{\Phi}^{S_i^{\iota\mathrm{r}}}\cdot\underline{\dot{\varphi}}^{S_i}\\ \delta\underline{\alpha}^{S_3} &= {}^{S_3}\bar{\Phi}^{S_1}\cdot\underline{\alpha}^{S_1} + \sum_{i=2}^{3} {}^{S_k}\bar{\Phi}^{S_i}\,.\,{}^{S_i}\bar{\Phi}^{S_i^{\iota\mathrm{r}}}\cdot\underline{\ddot{\varphi}}^{S_i}\end{aligned} \tag{58}$$

The 'internal transformation matrices' ${}^{S_i}\bar{\Phi}^{S_i^{\iota\mathrm{r}}}$ and ${}^{S_i}\bar{\Phi}^{S_i^{\iota\mathrm{t}}}$ for the angular and linear DOFs are obtained as (take $i=3$; see also the clarification after equation (22) in §2.1)):

$$\begin{aligned}{}^{S_3}\bar{\Phi}^{S_3^{\iota\mathrm{r}}} &= \left[\Phi_\mathrm{x}(\bar{\phi}_3^{S_3})\cdot\underline{\Phi}_{\mathrm{y}_3}(\bar{\phi}_2^{S_3}) \quad \underline{\Phi}_{\mathrm{x}_2}(\bar{\phi}_3^{S_3}) \quad \underline{e}_1\right]\\ {}^{S_3}\bar{\Phi}^{S_3^{\iota\mathrm{t}}} &= \left[\Phi_\mathrm{x}(\bar{\phi}_3^{S_3})\cdot\underline{\Phi}_{\mathrm{y}_3}(\bar{\phi}_2^{S_3}) \quad \underline{\Phi}_{\mathrm{x}_1}(\bar{\phi}_3^{S_3}) \quad \underline{e}_2\right]\end{aligned} \tag{59}$$

See for a detailed treatment of these matrices §4.3.1 in [19], specifically the equations 4.11, 4.12 and 4.37.

The bottom-up ranking of the angular DOFs is *torsion-foreaft-sideward*, so the $z-$, $y-$ and $x-$axis are the respective rotation axes. This implies that $\dot{\varphi}_1^{S_3}$ contributes just via the unit $x-$vector $\underline{e}_1$ to the rotational speed along the final coordinate system $\vec{e}^{\,S_k}_{(1,2,3)}$.

The second rotational speed increment, $\dot{\varphi}_2^{S_3}$ along the y-axis, contributes via the second column $\underline{\Phi}_{\mathrm{x}_2}(\bar{\phi}_3^{S_3})$ of the incremental transformation matrix along the x-axis. The second column applies because the rotation is along the y-axis; it concerns a column of the incremental transformation along the x-axis because the subsequent *third* bottom-up ranked rotation is along the x-axis. Similarly, the first bottom-up ranked rotation is multiplied with the *third* column of the incremental transformation matrix along the y-axis, and afterwards further transformed with incremental transformation along the x-axis.

Note that the linear DOFs associated with bending angular DOFs are along perpendicularly oriented axes. Thus, for the *second* translation $\dot{\underline{\varrho}}_2^{S_3}$, the *first* column of the transformation matrix along the x-axis applies in the expressions for ${}^{S_3}\bar{\Phi}^{S_3^{\iota\mathrm{t}}}$ since the y-axis rotation is accompanied by the x-axis translation, etc.

The expressions for the fed forward kinematic variables of the foundation element S_1 are:

$$\begin{aligned}\delta\underline{\omega}^{S_1} &= {}^{S_1}\bar{\Phi}^{S_1^{\iota\mathrm{r}}}\cdot\underline{\dot{\varphi}}^{S_1}\\ \delta\underline{\alpha}^{S_3} &= {}^{S_1}\bar{\Phi}^{S_1^{\iota\mathrm{r}}}\cdot\underline{\ddot{\varphi}}^{S_1}\end{aligned} \tag{60}$$

The expressions for the zero-mean linear velocity and acceleration in the centre of gravity of tower element S_3 are:

$$\delta\underline{v}^{S_3^*} = {}^{S_3}\bar{\Phi}^{S_1}\,\underline{v}^{S_1^\oplus} + \sum_{p=2}^{3} {}^{S_3}\bar{\Phi}^{S_p}\mathrm{J}^3_{v=1}\big({}^{S_p}\underline{\bar{\Phi}}_v^{S_1}\times{}^{S_p^\ominus}\underline{r}^{S_{p|3}^{\oplus|*}}\big)\,\underline{\omega}^{S_1} +$$

$$\sum_{i=2}^{3} {}^{S_3}\bar{\Phi}_v^{S_i^{\iota\mathrm{t}}}\,\underline{\dot{\varrho}}^{S_i} + \sum_{i=2}^{3}\sum_{p=i}^{3} {}^{S_3}\bar{\Phi}^{S_p}\mathrm{J}^3_{v=1}\big({}^{S_p}\bar{\Phi}_v^{S_i^{\iota\mathrm{r}}}\times{}^{S_p^\ominus}\underline{r}^{S_{p|3}^{\oplus|*}}\big)\,\underline{\dot{\varphi}}^{S_i}$$

$$\delta\underline{a}^{S_3^*} = {}^{S_3}\bar{\Phi}^{S_1}\,\underline{a}^{S_1^{\oplus}} + \sum_{p=2}^{3} {}^{S_3}\bar{\Phi}^{S_p}\,\mathrm{J}^3_{v=1}\big({}^{S_p}\bar{\underline{\Phi}}_v^{S_1} \times^{S_p^{\ominus}} \underline{r}^{S_{p|3}^{\oplus|*}}\big)\,\underline{\alpha}^{S_1} + \sum_{i=2}^{3} {}^{S_3}\bar{\Phi}_v^{S_i^{\iota t}}\,\underline{\ddot{o}}^{S_i} + \sum_{i=2}^{3}\sum_{p=i}^{3} {}^{S_3}\bar{\Phi}^{S_p}\,\mathrm{J}^3_{v=1}\big({}^{S_p}\bar{\Phi}_v^{S_i^{\iota r}} \times^{S_p^{\ominus}} \underline{r}^{S_{p|3}^{\oplus|*}}\big)\,\underline{\ddot{\varphi}}^{S_i} \tag{61}$$

with:

$$\begin{aligned} {}^{S_p}\bar{\Phi}_v^{S_i^{\iota r}} &= {}^{S_p}\bar{\Phi}^{S_i} \,.\, {}^{S_i}\bar{\underline{\Phi}}_v^{S_i^{\iota r}} \\ {}^{S_p}\bar{\Phi}_v^{S_i^{\iota t}} &= {}^{S_p}\bar{\Phi}^{S_i} \,.\, {}^{S_i}\bar{\underline{\Phi}}_v^{S_i^{\iota t}} \end{aligned} \tag{62}$$

The expressions for the fed forward kinematic variables of the foundation element S_1 are:

$$\begin{aligned} \delta\underline{v}^{S_1^{\oplus}} &= {}^{S_1}\bar{\Phi}_v^{S_1^{\iota t}}\,\underline{\dot{o}}^{S_1} + \mathrm{J}^3_{v=1}\big({}^{S_1}\bar{\Phi}_v^{S_1^{\iota r}} \times^{S_1^{\ominus}} \underline{r}^{S_1^{\oplus}}\big)\,\underline{\dot{\varphi}}^{S_1} \\ \delta\underline{a}^{S_1^{\oplus}} &= {}^{S_1}\bar{\Phi}_v^{S_1^{\iota t}}\,\underline{\ddot{o}}^{S_1} + \mathrm{J}^3_{v=1}\big({}^{S_1}\bar{\Phi}_v^{S_1^{\iota r}} \times^{S_1^{\ominus}} \underline{r}^{S_1^{\oplus}}\big)\,\underline{\ddot{\varphi}}^{S_1} \end{aligned} \tag{63}$$

Equations of motion

For element S_3 the equations of motion, expressed as normal differential vector equations along the coordinate system $\vec{e}^{\,S_3}_{(x,y,z)}$, then look like:

$$\begin{aligned} &{}^{S_3^{\ominus}}\underline{r}^{S_3^*} \times m^{S_3}\cdot\delta\underline{a}^{S_3^*} + \boldsymbol{I}^{S_3}\cdot\delta\underline{\alpha}^{S_3} = {}^{\mathrm{RS}}\underline{t}^{S_3^{\ominus}} + {}^{\mathrm{h}}\underline{t}^{S_3^{\mathrm{h}}} + \\ &\quad {}^{S_3^{\ominus}}\underline{r}^{S_3^{\mathrm{h}}} \times {}^{\mathrm{h}}\underline{f}^{S_3^{\mathrm{h}}} + {}^{S_3^{\ominus}}\underline{r}^{S_3^*} \times {}^{\mathrm{g}}\underline{f}^{S_3^*} + {}^{S_4^{\ominus}}\underline{t}^{S_3^{\oplus}} + {}^{S_3^{\ominus}}\underline{r}^{S_3^{\oplus}} \times {}^{S_4^{\ominus}}\underline{f}^{S_3^{\oplus}} \\ &m^{S_3}\cdot\delta\underline{a}^{S_3^*} = {}^{\mathrm{RS}}\underline{f}^{S_3^{\ominus}} + {}^{\mathrm{h}}\underline{f}^{S_3^{\mathrm{h}}} + {}^{\mathrm{g}}\underline{f}^{S_3^*} + {}^{S_4^{\ominus}}\underline{f}^{S_3^{\oplus}} \end{aligned} \tag{64}$$

The concentrated hydrodynamic forces are expressed similarly to the concentrated aerodynamic forces by equation (27), except that distributed torque loading is omitted and that matrix elements 'on z-axis locations' are shifted to 'y-axis locations':

$$\begin{aligned} {}^{\mathrm{h}}\underline{f}^{S_3^{\mathrm{h}}} &= \sum_{j=-1}^{1} {}^{\mathrm{h}}G^{\mathrm{F}}_{\mathrm{fq}_{3,j}} \,.\, {}^{S_3}\Phi^{H} \cdot \underline{q}_{\mathrm{f}}^{S_{3+j}^{\mathrm{h}}} \\ {}^{\mathrm{h}}\underline{t}^{S_3^{\mathrm{h}}} &= \sum_{j=-1}^{1} {}^{\mathrm{h}}G^{\mathrm{F}}_{\mathrm{tq}_{3,j}} \,.\, {}^{S_3}\Phi^{H} \cdot \underline{q}_{\mathrm{f}}^{S_{3+j}^{\mathrm{h}}} \end{aligned} \tag{65}$$

Morison's equation is adopted for the calculation of the hydrodynamic distributed loads; see [13]. Average loads may exist when water current is specified. Only the horizontal distributed hydrodynamic forces are consdired. This component is in the first location of vector $\underline{q}_{\mathrm{f}}^{S_3^{\mathrm{h}}}$.

With $\boldsymbol{C}_{\mathrm{V}}^{S_k}$ and $\boldsymbol{C}_{\mathrm{M}}^{S_k}$ the 'hydrodynamic viscous and mass coefficient matrices', given by

$$\boldsymbol{C}_{\mathrm{V}}^{S_3} = \begin{pmatrix} C_{\mathrm{V}}^{S_3^{\mathrm{h}}} & 0 & 0 \\ 0 & 0 & 0 \\ 0 & 0 & 0 \end{pmatrix} \;;\; \boldsymbol{C}_{\mathrm{M}}^{S_3} = \begin{pmatrix} C_{\mathrm{M}}^{S_3^{\mathrm{h}}} & 0 & 0 \\ 0 & 0 & 0 \\ 0 & 0 & 0 \end{pmatrix} \tag{66}$$

the following expression holds for the coordinate vector $\underline{q}_{\mathrm{f}}^{S_3^{\mathrm{h}}}$:

$$\begin{aligned} \underline{q}_{\mathrm{f}}^{S_3^{\mathrm{h}}} &= \tfrac{1}{2}\rho_{\mathrm{H}}\cdot D^{S_3^{\mathrm{h}}}\cdot\boldsymbol{C}_{\mathrm{V}}^{S_3}\cdot(|\underline{w}^{S_3^{\mathrm{h}}}|.\times\underline{w}^{S_3^{\mathrm{h}}}) + \\ &\quad \tfrac{1}{4}\rho_{\mathrm{H}}\cdot\pi(D^{S_3^{\mathrm{h}}})^2\cdot\boldsymbol{C}_{\mathrm{M}}^{S_3}\cdot\dot{\underline{w}}^{S_3^{\mathrm{h}}} \end{aligned} \tag{67}$$

The '. × ' operation means 'element by element' regular multiplication.

For the relative wave speed and wave acceleration vector hold:

$$\begin{aligned} \underline{w}^{S_3} &= \begin{bmatrix} w_{\mathrm{horz}}^{S_3^{\mathrm{h}}} \\ 0 \\ 0 \end{bmatrix} - {}^{H}\Phi^{S_3}\cdot\underline{v}^{S_3^{\mathrm{h}}} \\ \dot{\underline{w}}^{S_3} &= \begin{bmatrix} \dot{w}_{\mathrm{horz}}^{S_3^{\mathrm{h}}} \\ 0 \\ 0 \end{bmatrix} - \frac{C_{\mathrm{M}}^{S_3^{\mathrm{h}}}-1}{C_{\mathrm{M}}^{S_3^{\mathrm{h}}}}\cdot{}^{H}\Phi^{S_3}\cdot\underline{a}^{S_3^{\mathrm{h}}} \end{aligned} \tag{68}$$

The horizontal wave speed w_{horz} and acceleration $\dot{w}_{\mathrm{horz}}$ pertain to the underwater level for hydrodynamic conversion point S_3^{h} and follow from the wave spectrum and the dispersion relation; see §10.3 in [19]. The hydrodynamic load is also affected by the tower speed $\underline{v}$ and tower acceleration $\underline{a}$ in the point S_3^{h}.

Matrix ${}^{S_3}\Phi^{H}$ transforms coordinates along $\vec{e}^{\,H}$ to coordinates along the 'structural tower element coordinate system' $\vec{e}^{\,S_3}$ with co-axial z-axis; the x- and y-axis of $\vec{e}^{\,S_3}$ coincide with the neutral (bending-)elastic axes for sideward and foreaft oriented tower deformation. The matrix depends on soil compliance and tower deformation, and on the orientation difference between the waves and the tower base.

The gravity loading ${}^{\mathrm{g}}\underline{f}^{S_3^*}$ consists of mean loading and variation due to change of orientation by tower deformation. The linearised expression is:

$$ {}^{\mathrm{g}}\underline{f}^{S_3^*} = {}^{\mathrm{g}}\bar{\underline{f}}^{S_3^*} + \frac{\partial^{\mathrm{g}}\underline{f}^{S_3^*}}{\partial\underline{g}_{\mathrm{ori}}^{S_1}}\cdot\delta\underline{g}_{\mathrm{ori}}^{S_1} + \frac{\partial^{\mathrm{g}}\underline{f}^{S_3^*}}{\partial\underline{\phi}^{S}}\cdot\delta\underline{\phi}^{S} \tag{69}$$

For the sensitivities $\partial^{\mathrm{g}}\underline{f}^{S_3^*}/\partial\underline{g}_{\mathrm{ori}}^{S_1}$ and $\partial^{\mathrm{g}}\underline{f}^{S_3^*}/\partial\underline{\phi}^{S}$ holds:

$$\begin{aligned} \frac{\partial^{\mathrm{g}}\underline{f}^{S_3^*}}{\partial\underline{g}_{\mathrm{ori}}^{S_1}} &= m^{S_3}\,.\,{}^{S_k}\bar{\Phi}^{S_1} \\ \frac{\partial^{\mathrm{g}}\underline{f}^{S_3^*}}{\partial\underline{\phi}^{S}} &= [\mathbf{O}_{(1)}\ \ \ldots \\ &\quad \mathrm{J}^k_{i=2}\Big(\mathrm{J}^3_{v=1}\big(\frac{\partial^{S_3}\Phi^{S_0}}{\partial\phi_v^{S_i}}\cdot{}^{B}\underline{\Phi}^{G}_{3}\cdot m^{S_3}\cdot\mathrm{g}\big)\Big)\ \mathbf{O}_{(4\ldots M)}] \end{aligned} \tag{70}$$

For the feedthrough gravity variation $\delta \underline{g}_{\mathrm{ori}}^{S_1}$ holds

$$\begin{aligned} \delta \underline{g}_{\mathrm{ori}}^{S_1} &= \sum_{v=1}^{3} \frac{\partial^{S_1}\Phi^{S_0}}{\partial \phi_v^{S_1}} \cdot {}^{B}\underline{\Phi}_3^{G} \cdot \mathrm{g}\delta\phi_v^{S_1} \\ &\text{with } {}^{B}\Phi^{G} = \Phi_{\mathrm{y}}(-\theta^{B}) \cdot \Phi_{\mathrm{z}}(\gamma^{B}) \end{aligned} \tag{71}$$

The angles θ^B and γ^B define the orientation of the wind turbine base B relative to the geographic coordinate system that corresponds with the compass.

The responsive loads ${}^{\mathrm{RS}}\underline{t}^{S_k^{\ominus}}$ and ${}^{\mathrm{RS}}\underline{t}^{S_k^{\ominus}}$ in the tower elements S_2 up to S_{M-1} are identically expressed in DOFs as those in the blade profile & structure elements.

The responsive loads ${}^{\mathrm{RS}}\underline{f}^{S_1^{\ominus}}$ and ${}^{\mathrm{RS}}\underline{t}^{S_1^{\ominus}}$ in the foundation element may be explicitely specified by spring and damper constants, including cross coupling terms for coupled linear and angular terms in a bending direction, just as for the rotor shaft & hub. TURBU also facilitates the automatic calculation of (cross coupled) springs in the mounting point of the wind turbine (entry point $S_1^{\ominus}$) based on under ground tower extension. The expressions for the responsive loads are similar to those in the rotor centre by equation (57).

A.4 Wake equations

Consider a rotor annulus which coincides with the track made by three corresponding elements of the rotor blades. The 'equations of equilibrium' correspond to those adopted by Lindenburg and Schepers in [16]. Herein is assumed that only the lift forces contribute to the setting of the aerodynamic equilibrium. The equation for the axial and tangential induction speed U_{i} and V_{i} then looks like (number of blades $B = 3$):

$$\begin{aligned} \tfrac{1}{2}\rho C_{\mathrm{L}}(\phi_{\mathrm{a^{\circ}}})cS \cdot U_{\ell}\cos\beta\sqrt{U_{\mathrm{n}}^2 + U_{\ell}^2} &= \tfrac{2\pi}{B}\rho r \cdot \Delta r\, \bar{F}_{\mathrm{p}} 2U_{\mathrm{i}}U_{\mathrm{tr}} \\ \tfrac{1}{2}\rho C_{\mathrm{L}}(\phi_{\mathrm{a^{\circ}}})cS \cdot U_{\mathrm{n}}\sqrt{U_{\mathrm{n}}^2 + U_{\ell}^2} &= \tfrac{2\pi}{B}\rho r\, \Delta r\, \bar{F}_{\mathrm{p}} 2V_{\mathrm{i}}U_{\mathrm{tr}} \end{aligned} \tag{72}$$

In here U_{tr} represents the transportation speed and $\bar{F}_{\mathrm{p}}$ Prandtl's correction factor.

Transportation speed U_{tr} is the vector sum of the axial, lateral and vertical wind speed in the rotor annulus; the axial speed is diminished with the axial induction. In dynamic conditions the average over the wind speeds on the three blade elements that rotate in the annulus are considered for the determination of U_{tr}. Prandtl's correction factor $\bar{F}_{\mathrm{p}}$ accounts for both tip and root effects. The expressions for U_{tr} and $\bar{F}_{\mathrm{p}}$ are generally known and can a.o. be found in [11], [16] and [20].

The point of departure for the linearised model for the induction transients is based on the following formulation of the ECN Differential Equation model:

$$\begin{aligned} \tfrac{\mathrm{d}}{\mathrm{d}t}\left(U_{\mathrm{i_m}}^{W_3}\right) = &-\frac{U_{\mathrm{i_m}}^{D_3}U_{\mathrm{tr}}^{D_3} + U_{\mathrm{i_m}}^{E_3}U_{\mathrm{tr}}^{E_3} + U_{\mathrm{i_m}}^{F_3}U_{\mathrm{tr}}^{F_3}}{B \cdot R \cdot \mathcal{F}_{\mathrm{a}}^{W_3}} - \\ &\frac{\left({}^{\mathrm{a_L}}f_1^{D_3} + {}^{\mathrm{a_L}}f_1^{E_3} + {}^{\mathrm{a_L}}f_1^{F_3}\right)}{\rho 2\pi r^{W_3}\Delta r^{W_3} \cdot 2R \cdot \mathcal{F}_{\mathrm{a}}^{W_3}\left(\frac{F^{D_3}+F^{E_3}+F^{F_3}}{B}\right)} \end{aligned} \tag{73}$$

with:

$$\mathcal{F}_{\mathrm{a}}^{W_3} = \frac{2\pi}{\displaystyle\int_0^{2\pi}\left\{\frac{1 - \left(r^{W_3}/R\right)\cos\psi}{\left[1 + \left(r^{W_3}/R\right)^2 - 2\left(r^{W_3}/R\right)\cos\psi\right]^{1.5}}\right\}\mathrm{d}\psi} \tag{74}$$

The lift force reactions ${}^{\mathrm{a_L}}f_1^{X_k}$ by the blades, along the x-axis of the annulus coordinate systems, correspond with the left hand term in the axial equilibirum equation (72) with a minus sign.

Here the 3rd rotor annulus is considered, which coincides with the track made by blade elements D_3, E_3 and F_3.

This formulation establishes a clear interface with the structural and quasi-steady aerodynamic blade submodels in accordance with figure 2. In addition, it accounts for the influence of blade-individual flow conditions, although this is limited to affection of the assumed annulus-uniform induction.

TURBU facilitates to specify the number of blade elements as an integer muliplite of the rotor annuli, in that case the lift reaction forces are summed over all blade elements within an annulus.